University of Cambridge
Department of Engineering

Vibration of Prestressed Membrane Structures

Dissertation submitted to the University of Cambridge
for the Degree of Master of Philosophy

by

S. Kukathasan

Churchill College

August 2000

Declaration

The author wishes to declare that, except for commonly understood ideas and concepts, or where specific reference is made to the work of other authors, the contents of this dissertation are original and include nothing that is the outcome of work done in collaboration with others. The research described in this dissertation has been carried out in the Department of Engineering at the University of Cambridge from October 1999 to August 2000. This dissertation has not previously been submitted, in part or whole, to any other university or institution for any degree, diploma, or other qualification. This is presented in approximately 14,900 words excluding bibliography and appendix.

S. Kukathasan

Acknowledgements

First and foremost, I would like to thank my supervisor Dr. S. Pellegrino for his help, guidance and encouragement throughout my research. His insight and enthusiasm have helped me to make my work a success. Also I would like to thank Professor J. Woodhouse and Dr. W. R. Graham for many helpful suggestions and discussions.

I would like to thank Mr. Roger Denston and Mr. Peter Knott for their technical assistance, to Dr. Arul Britto and Mr. Paul Bayford for their computing assistance. Also, I thank Mrs. Margaret Cosnett and other engineering library staff for their help in the library.

I would like to thank all members of the Structures Research Group for their friendship and helpful discussions. My special thanks go to Gunnar Tibert, Jason Lai and Khuram Iqbal for their invaluable help in computing.

I am very grateful to Michael Turton, my college friend, for his unflagging help and friendship. Also I should thank Byron and Caroline for their help and friendship in my college.

Financial support from the Cambridge Commonwealth Trust, Matra Marconi Space and the Department of Engineering is gratefully acknowledged.

Abstract

Large deployable space structures include requirements for reflecting surfaces for antennae, reflectors and solar arrays. Their efficiency depends not only on surface accuracy but also on the vibration characteristics of these reflecting surfaces. This dissertation presents a study of the vibration behaviour of various prestressed membrane structures.

A preliminary vibration analysis of arbitrary shape flat membranes is done using a finite element package, ABAQUS, and compared with analytical solutions. The preliminary analysis shows good agreement between finite element and analytical solutions. This gave confidence to use ABAQUS simulations for vibration analysis of other membrane structures as well.

The natural frequencies and mode shapes of a deployable membrane reflector currently under development by the European Space Agency are obtained using ABAQUS for various reflector diameters, hub dimensions, number of ribs and prestress. The analysis results indicate that the fundamental natural frequency of the reflector decreases with the increase of diameter of the reflector and does not change greatly with the increase of hub radius. Furthermore, the fundamental natural frequency increases with the increase of membrane prestress. A periodic nature of variation in the results is observed.

An experimental study of the vibration of a flat membrane is done. The experimental results indicate the effect of the surrounding air on the membrane vibration. A similar experimental study carried out at various atmospheric pressures in a vacuum chamber, published in 1983, is used to study the effect of the surrounding medium on the membrane vibration. A new prediction method is presented to determine the natural frequencies and mode shapes of flat membranes of any shape vibrating in a fluid medium at any pressure.

Contents

List of Figures

List of Tables

Chapter 1

Introduction

1.1 Membrane Structures

Membrane structures consist of thin membrane or fabric as a major structural element. A membrane has no compression or bending stiffness, therefore it has to be prestressed to act as a structural element. Major applications of membrane structures occur mainly in large span lightweight roof structures, temporary buildings such as tents and shelters. The analysis, design and construction of such structures is a field that has developed very considerably during the last 30 years.

The type of structures that is of interest in the present study is high-precision deployables for spacecraft, where is a growing requirement for furlable reflecting surfaces for antennae, reflectors and solar arrays. The configurations that are being considered include flat prestressed membrane panels and paraboloidal prestressed membranes formed by contiguous cylindrical pieces. The performance efficiency of these reflective surfaces depends not only on the geometric accuracy of the surface but also on its vibration characteristics.

The vibration of lightweight structures are affected considerably by the surrounding medium. Thus, spacecraft structures should be tested in a vacuum chamber, but this would be too costly for a large structure. This dissertation explains ways of using experimentally validated simulation methods to deal with this problem.

1.2 Scope of the Dissertation

The aim of this dissertation is to develop methods for predicting the vibration behaviour of prestressed membrane structures of general shapes, with a thickness of only a fraction of a millimetre. Numerical and experimental studies of the

vibration of flat membranes provide a natural way of approaching this field. The results obtained indicate that the surrounding medium has significant effects on the vibration of ultra-thin membranes. Structure-air interaction effects are studied. An analytical method to predict the natural frequency and mode shape of a membrane vibrating in air is derived. Results from this prediction method are compared to the results of an extensive experimental study by Sewall et al. [35], plus experiments in air done by the author. Some of the predictive methods developed in the course of this study are applied to predict the in-orbit vibration behaviour of Collapsible Rib Tensioned Surface (CRTS) Reflectors.

1.3 Layout of the Dissertation

The layout of this dissertation is as follows. Chapter 2 gives a brief overview of the previous work in the area of deployable structures, CRTS Reflectors and periodic structures. Previous work on air-structure interaction problems is briefly reviewed.

Chapter 3 is a numerical and analytical study of simple flat membranes plus a simple structure consisting of membrane elements. The modelling of prestressed membrane structures in ABAQUS is explained, including the selection of appropriate elements in ABAQUS. The finite element results are compared to available analytical results for simple membranes and different ways of modelling the membrane, e.g. as a grid of truss elements, are considered.

Chapter 4 presents a numerical study of CRTS reflectors. Estimates of the in-vacuum vibration of CRTS reflectors are obtained and, since no experimental results are currently available, the finite element analysis results obtained using continuum membrane elements are compared to a truss element model.

Chapter 5 describes an experiment carried out on a triangular-shaped membrane with inwardly curved edges, tensioned by thin cables along the edges. The experiment used a laser vibrometer to determine the natural frequencies and a loudspeaker arrangement to obtain the mode shapes and confirm the natural frequency measurements. The results of a numerical analysis of natural frequencies and mode shapes are compared to the experimental measurements.

Chapter 6 deals with air-structure interaction effects. A simple prediction method for the natural frequencies and mode shapes in different air pressures is proposed. The above method is checked against the experimental study done by Sewall et al. [35]. The method is also applied to predict the experimental measurements presented in Chapter 5.

Chapter 7 concludes the report and identifies further work that needs to be done in this area.

Chapter 2

Literature Review

This chapter reviews previous work relevant to this dissertation. Section 2.1 gives a brief outline of work in the deployable structures field that are relevant to this study. Section 2.2 explains the concept in CRTS Reflector and previous related work. Because of the periodic nature of CRTS reflectors, vibration and mode localisation phenomena in periodic structures are briefly reviewed in section 2.3. Section 2.4 gives a brief overview of previous work in the area of air-structure interaction.

2.1 Previous Work on Deployable Structures

Deployable structures are a special type of structures, which can be packaged for transportation and expanded automatically in the desired place. They differ from conventional engineering structures, because they are built to undergo very large geometric deformation and transformation. Two types of deployable structures, membrane structures and thin-walled structures, are briefly reviewed in this section. The purpose of this review is to show the importance of vibrational analysis on the membrane and thin-walled structures. The vibrational analysis is carried out in the following chapters.

(a) Membrane Structures

Membranes, which are a special type of deployable structures, do not have any in-plane stiffness when the applied tension is removed. The major advantage of using membranes in deployable structures is that they can be packaged in any arbitrary pattern and expanded while in orbit. Also, membranes are inexpensive and lightweight source of materials compared with other feasible materials. They are mainly used in solar arrays, inflatable antennae and reflectors.

Solar arrays and reflectors are important components of satellites. Figure 2.1(a) shows the *Mars Express—Orbiter* satellite (to be launched in 2003 by European Space Agency (ESA)), which uses solar arrays to provide power requirements and reflectors for communications and astronomy observations. In the satellite, the solar arrays are stored in a folded form when it is launched and expanded when supportive structures are deployed once in orbit. In the solar array, flat membranes are stretched between each panels, and the each panel is connected by foldable ribs.

(a) Mars Express—Orbiter. (b) Hubble Telescope.

Figure 2.1: Membrane structures (Courtesy of ESA).

Figure 2.1(b) is the Hubble telescope which uses solar arrays to provide power requirements. This solar array is similar to the above one, i.e. solar panels are stored in a folded form when it is launched and expanded once in orbit.

The another new concept for the deployable solar array is shown in Figure 2.2. Here, membrane is rolled up when the solar array is packaged, and it is deployed when the stiff edge structure formed by the two booms is moved apart. A biaxial stress distribution in the membrane is achieved by choosing suitable parabolic shapes for the edges of the membrane.

Inflatable deployable space structures are used to gather more definite information on earth's environment and on other galaxies. A new class of these structures is the Inflatable Antenna Experiment (IAE) (launched in 1996 by NASA) shown in Figure 2.3. The IAE is an inflatable antenna 14 m in diameter mounted on three 28 m struts. The reflective surface was formed by the upper side of the canopy; which had the shape of an offset paraboloid with a focal length of 14 m and was made of 6.5 μm thick mylar. The lower part, also made of mylar, had the same

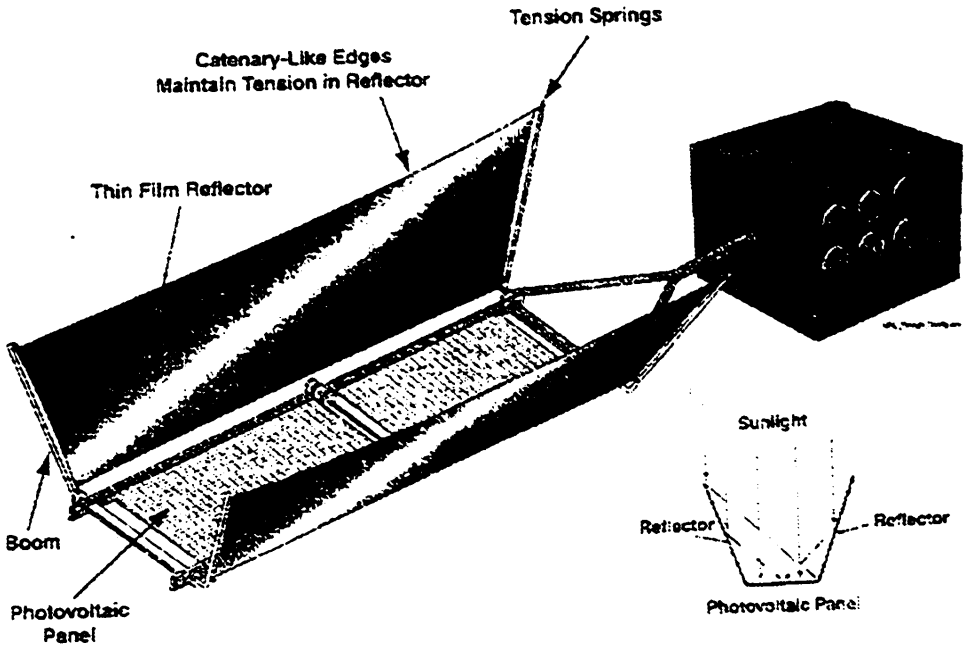

Figure 2.2: New concept for deployable solar array (from Miura and Pellegrino [28]).

shape. The canopy was inflated to a pressure of 4×10^{-5} bar, and was supported at the edge by a torus with a cross-sectional diameter of 610 mm, made of 0.28 mm thick Kevlar-reinforced Neoprene-rubber inflated to 0.14 bar. The struts had a diameter of 460 mm, were also made of the same material of the torus, and inflated to the same pressure.

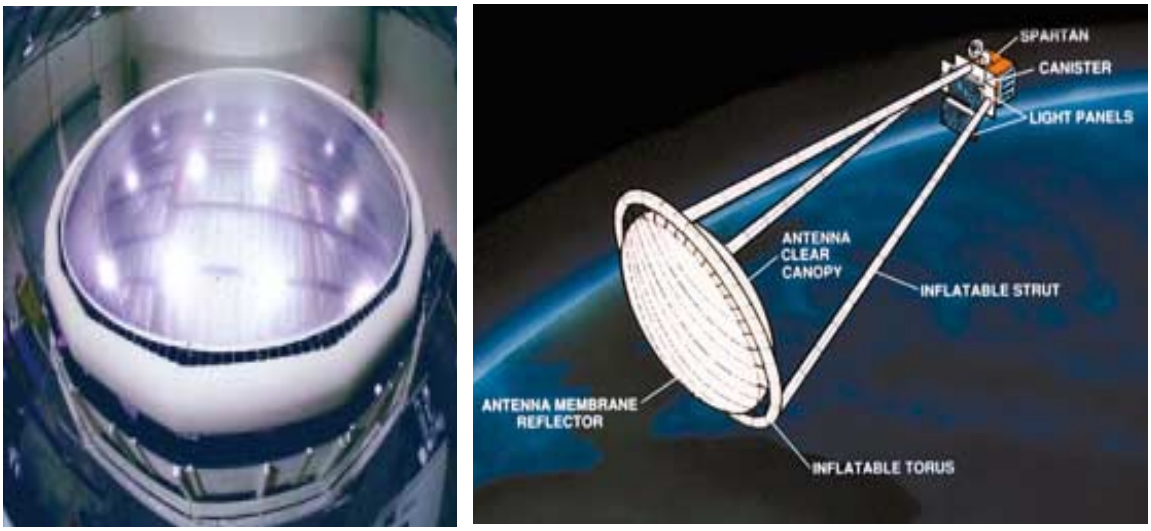

(a) Ground test. (b) Flight test.

Figure 2.3: Inflatable Antenna Experiment (Courtesy of L'Garde Inc.).

It can be observed from the above review that membrane structures have larger surface areas, they are lightweight and relatively flexible. Lightweight structures are preferred, as to achieve a low-cost structure the structural weight must be kept to a minimum. The efficiency and stability of the membrane structures depends on their dynamic controls in the deployed configuration, thus it is necessary to have a detailed understanding of vibration characteristics of these membrane structures.

(b) Thin-Walled Structures

Thin-walled structures are mainly used in membrane structures as connecting elements or supportive elements. For example, they are used as connecting elements in the solar array shown in Figure 2.1(a) and as supportive elements in the solar array shown in Figure 2.2. A steel tape measure, a thin-walled cylindrical shell whose cross-section forms an arc of a circle, is a well-known example of a thin-walled deployable structure. The Storable Tubular Extensible Member (STEM) is a simple extension of steel tape measure. The STEM has major applications on spacecraft. The STEM is formed from a thin sheet of metal, which is heat treated into a circular overlapped cross-section as shown in Figure 2.4(a). A variant on the STEM is the Bi-STEM shown in Figure 2.4(b) consisting of two STEM's—one nested inside the other. The main advantages of the Bi-STEM over the STEM are that (i) its rolled up width, as well as the length of the transition region between the rolled up and the extended regions, are smaller, and (ii) its symmetric construction makes its structural response more symmetric.

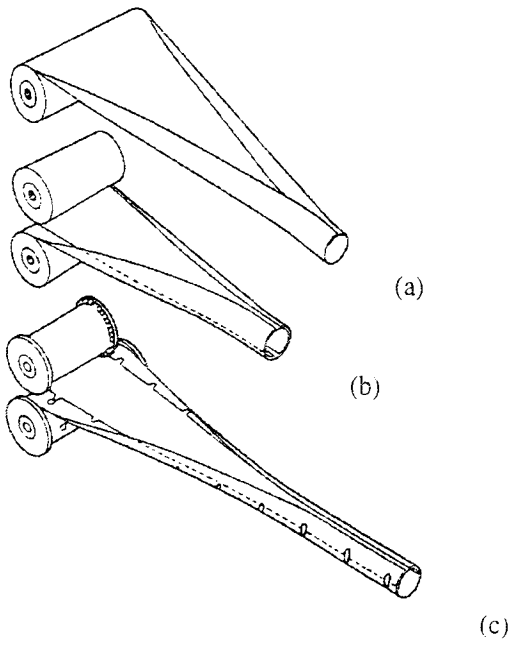

Figure 2.4: Family of STEM types: (a) STEM; (b) Bi-STEM; (c) zippered Bi-STEM (from King [21]).

Collapsible ribs are structurally similar to the tape measure. It is formed by bonding of two preformed tapes, each forming half of the cross-section of the tube as shown in Figure 2.5(a). It can be flattened and rolled up in a similar way to the STEM. The main advantage of this last scheme over the previous two concepts is that the collapsible tube has much higher torsional stiffness. Major applications of collapsible ribs are in the CRTS reflectors, and on spacecraft as shown in Figure 2.5(b).

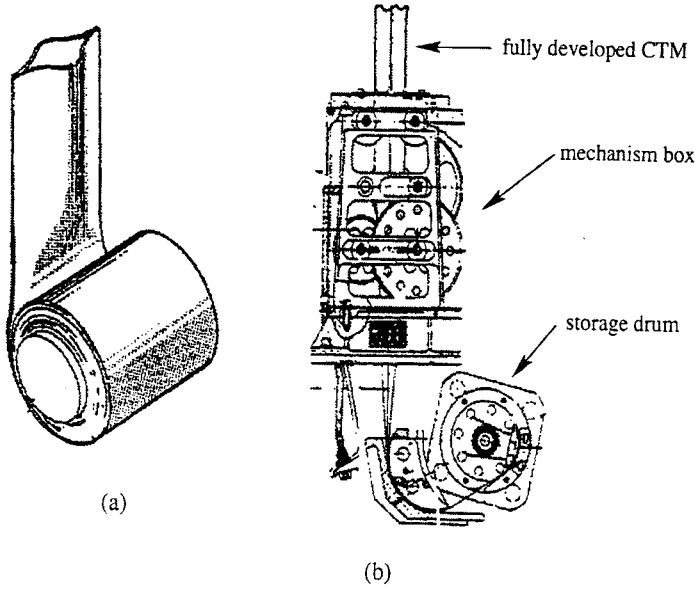

Figure 2.5: Collapsible rib: (a) cross-section profile; (b) application on spacecraft (from King [21]).

2.2 CRTS Reflector

Large space-based deployable reflectors are needed for a variety of different applications that include mobile communications, earth-observation radiometry, active microwave sensing and defence space-based radar. However, reflector user resources are so stringent that the result is a real need for low-cost, large-size, light-weight, and reliable deployable space reflector structures.

A concept of a multipurpose deployable reflector, called the Collapsible Rib Tensioned Surface (CRTS) reflector, is being developed by the European Space Agency. A CRTS reflector shown in Figure 2.6 consists of three main parts: a central expandable hub, a series of thin-walled foldable ribs connected radially to the hub and a membrane that is supported and tensioned by the ribs.

In the case of a symmetric reflector, the membrane consists of identical flat gores bonded together along their curved edges. When the reflector is deployed, each gore takes approximately the shape of a singly-curved cylindrical surface. The

Figure 2.6: CRTS Reflector.

overall shape of a CRTS reflector is not an exact paraboloid but only an approximation of it, the accuracy of which improves as the number of gores is increased. Each rib consists of a thin slender metal blade with curved cross section. A key feature of this structural element is that it is continuous, and yet it can be folded elastically in many different ways.

The packaging and deployment of CRTS reflectors have been studied, and three different packaging schemes have been implemented [40]. Figure 2.7 shows one of the packaging schemes of CRTS reflectors. In this scheme, each rib is folded alternately up and down, in a zig-zag shape, and the membrane is packaged between the ribs in a compatible way with the adjacent ribs. The latest development in CRTS reflector aimed on the shape accuracy and stress distribution in the deployed configuration of CRTS reflectors [23, 24]. The vibration characteristics of the CRTS reflector on its deployed configuration is analysed in Chapter 4.

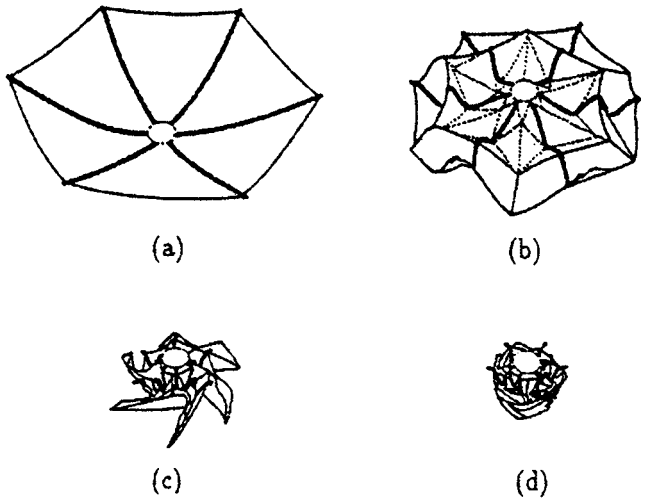

Figure 2.7: Packaging of a CRTS reflector (from King [21]).

2.3 Periodic Structures

Periodic structures consist of a number of identical repetitive units linked in a similar pattern. Many complex engineering structures can be included in this category. The analysis of these structures can be simplified by considering their periodic nature. Because of the periodic nature of the CRTS reflector, previous work on the vibration analysis of periodic structures is briefly reviewed below.

Figure 2.8 shows the natural frequency estimation of an infinite periodic beam from its wave propagation relationship, which studied by SenGupta [33,34].

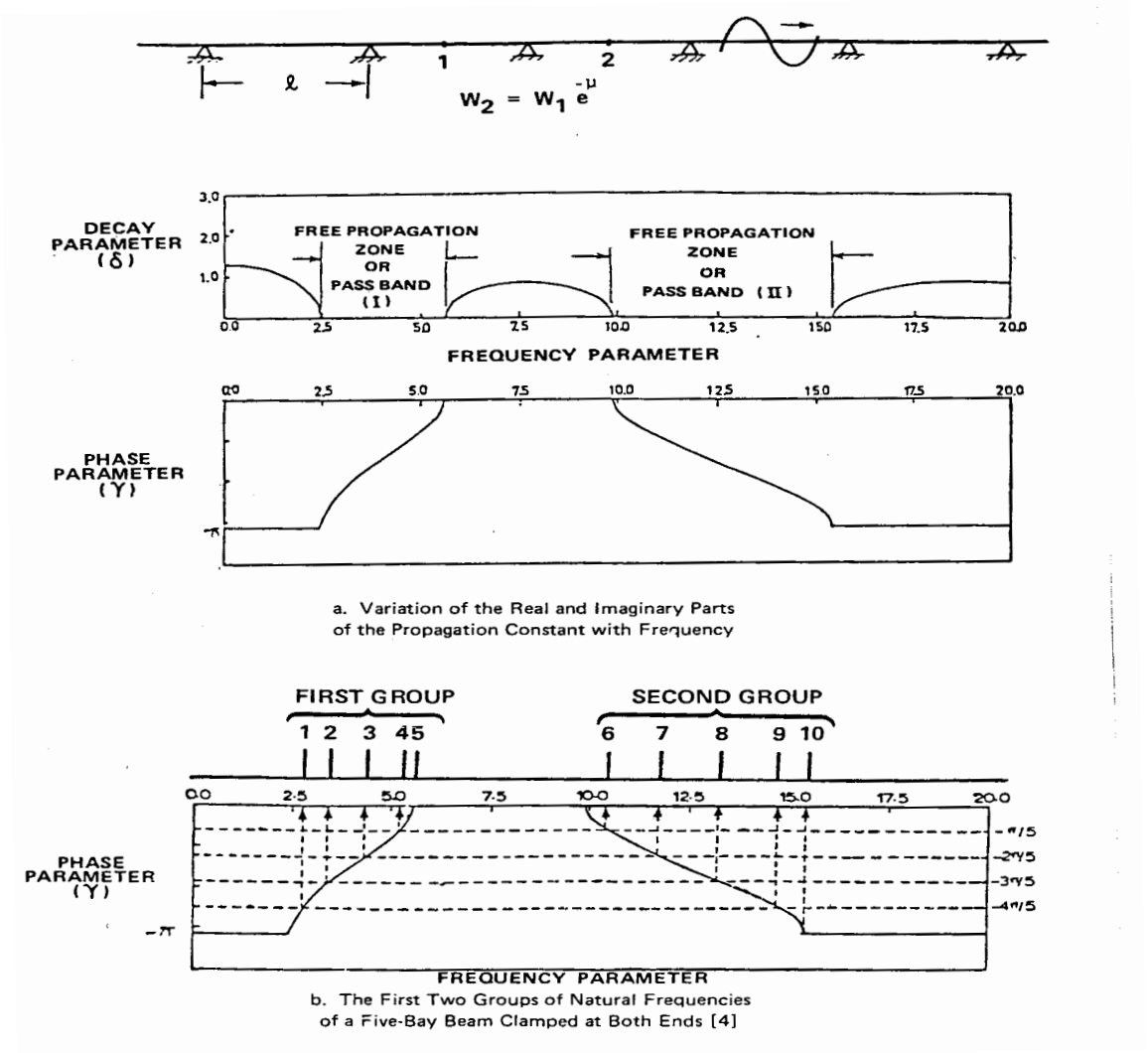

Figure 2.8: Natural frequencies of periodic beam (from SenGupta [34]).

For a flexural wave travelling from one bay to the next, the amplitudes at two points separated by a periodic distance can be related as

$$W_2 = W_1 e^{-\mu} \tag{2.1}$$

where μ is the propagation constant which is generally complex. The real part δ defines the rate of decay of the amplitudes from one support to the other and the imaginary part γ denotes the phase difference between the quantities at two successive supports.

Figure 2.8.a shows a typical propagation constant vs. frequency parameter plot for a periodically supported infinite beam.

The calculation of natural frequencies of a five-span beam clamped at both ends is explained as follows. By applying boundary conditions in the bending moment equation at the end supports, γ is obtained as [33]

$$\gamma = \frac{m\pi}{N} \tag{2.2}$$

where m is an integer which varies from 1 to N and N is total number of spans, i.e. in this case N=5.

Figure 2.8.b gives the natural frequency results of first two groups of the five-span beam. The results are obtained from Equation (2.2) and Figure 2.8.a. An important feature of this results is that the number of normal modes (or natural frequencies) in a given propagation zone (or in a group) is equal to the number of spans. The natural frequencies of a beam with N-spans can similarly be obtained from the same figure of γ vs. frequency parameter, by dividing the ordinate into N equal parts and reading the corresponding projections on the abscissa.

As explained above, periodic structures have the advantage of simplifying the dynamic analysis. But in reality, almost every practical structures have small irregularities because of manufacturing and material tolerances. The structural irregularities can affect the vibration behaviour of nearly periodic structures significantly by localising the vibration modes and confining the energy to a region close to the source. This phenomena is generally called mode localisation.

The mode localisation of a 15 m diameter space reflector with various number of ribs has been investigated numerically by Cornwell and Bendiksen [4]. In their study, the 18-ribs reflector did not localise in the first mode but the other higher modes did, and the localisation became progressively more severe with increasing mode number. When the number of ribs was increased to 48, the localisation became even more severe. This indicates the importance of considering mode localisation on a large space reflector having many number of ribs. More recent references in the area of mode localisation and energy confinement can be found in Yap and Cebon [38].

2.4 Air-Structure Interaction

An elastic structure in contact with an infinite fluid medium during its vibration induces the vibration of the surrounding fluid medium. When the wavelength of the fluid medium (acoustic wavelength) is larger than the structural wavelength, surface pressure on the structure due to vibration of the fluid medium can be specified as inertia forces. This effect can be simply explained as an additional mass due to a certain thickness of fluid layer on the structure. In this case, the fluid medium is assumed to be incompressible and the specified thickness of the fluid moves around the structure. As structures become larger and lighter, the effect of fluid mass becomes more important in predicting their natural frequencies and mode shapes. The analytical approach is reviewed in section 2.4.3 and Chapter 6.

2.4.1 Sewall et al.'s Model

A modal study of an ultra-lightweight flat membrane shown in Figure 2.9 done by Sewall et al. [35] shows the effect of air in the membrane vibration. This investigation gives the natural frequencies and the corresponding mode shapes of an experimental study carried out in a vacuum chamber in different air pressures, i.e. in vacuum, 0.61 atm and 1 atm. In this study, the membrane model was excited by an electrodynamic shaker attached to the cable leading from the lowest apex, and dynamic responses were measured using a deflectometer. Also, this study presents the results of a numerical analysis carried out using SPAR finite element package. The results of this experimental study indicate significantly lower and more closely spaced natural frequencies at higher pressures, with mode shapes more distorted than in vacuum. Also, an alteration in the sequence of identifiable modes is observed in this study.

An analytical approximation method is presented to simulate the air effect on the model in the study as follows. The effects of air on membrane vibration modes were approximated as a non structural mass contained in a curved envelope surface defined over a plane surface of the membrane as shown in Figure 2.10. The envelope surface is the locus of quarter circles lying in vertical planes normal to the membrane edge. The radius r_i of each quarter circle is the distance from the membrane edge to the nearest of the three symmetry axes. In each vertical plane, the element centroid is located by the coordinate ξ_i which, together with r_i, determines the distance z_i of the envelope surface from the membrane. The corresponding local mass per unit area m_i was computed and input to the SPAR package for vibration analysis as non-structural mass.

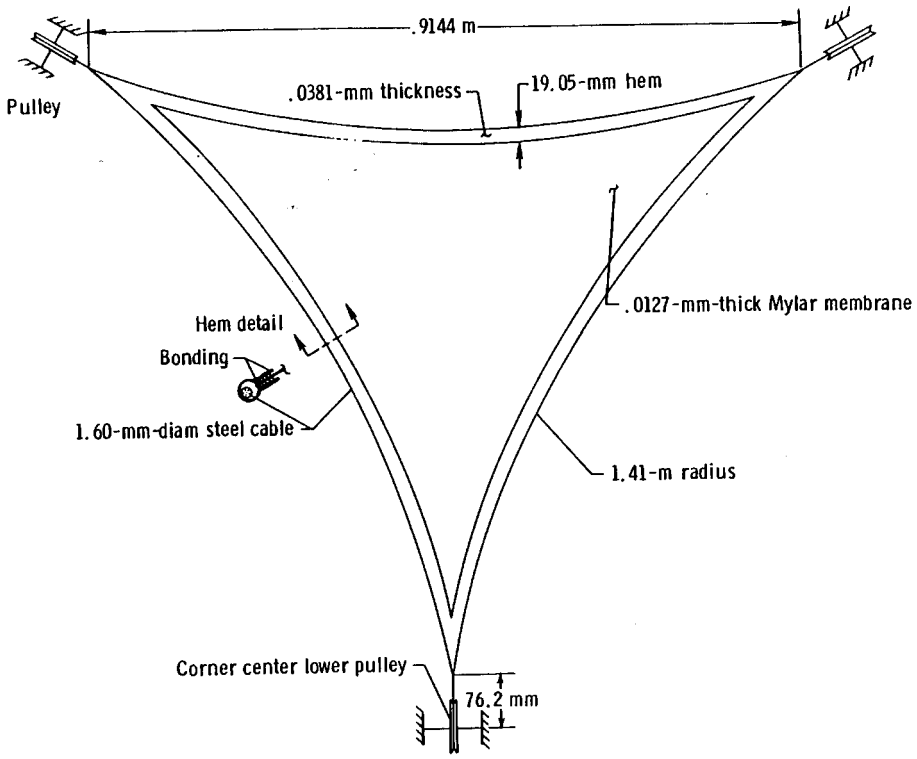

Figure 2.9: Sewall et al.'s membrane model (from Sewall et al. [35]).

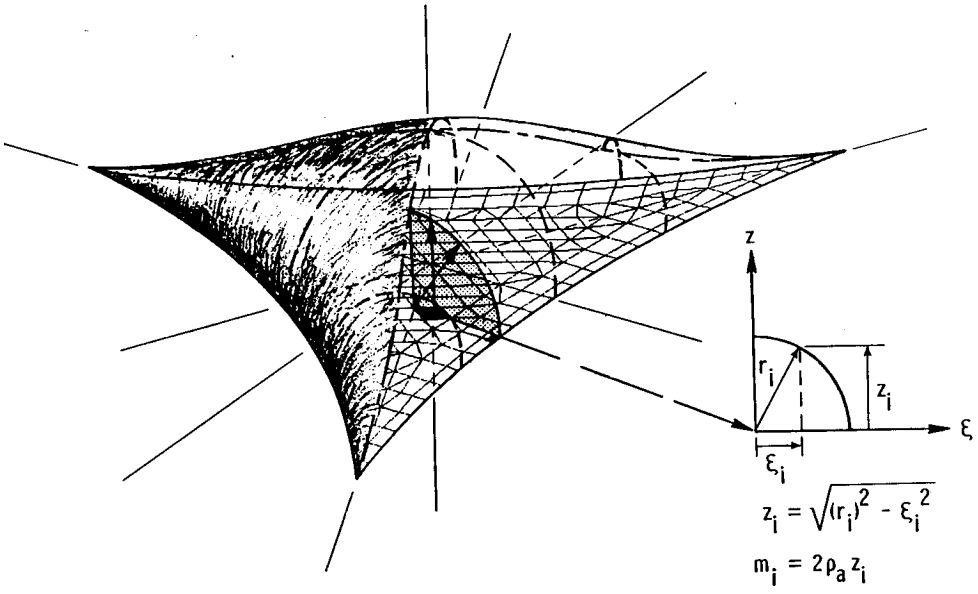

Figure 2.10: Air-mass approximation for Sewall et al.'s membrane model (from Sewall et al. [35]).

The method was not capable of predicting all the natural frequencies and the mode shapes accurately, in air. In higher modes, discrepancies in natural frequencies up to 27% are observed even for identifiable modes. There are several

reasons for the lack of agreement between the experimental and the approximation method. First, the method considered the same air mass for each mode, however, in reality, the air mass participating in the membrane vibration reduces with the increase of mode number. Therefore, a lower value of air mass has to be used for higher modes. Second, the air mass volume participating with the membrane was assumed arbitrarily. Therefore an alternative approximate analytical method is considered by the author. The experimental results is used in Chapter 6 to validate the alternative analytical method implemented by the author.

2.4.2 Numerical Methods

The air-structure interaction problem is a coupling problem between the air and its structural boundary. This coupled problem can be solved by combining a finite element model of the structure with a model of the air, computed using the finite element or boundary element or boundary integral method.

In the case of a fully submerged structure vibrating in an infinite fluid medium, a finite element representation of the fluid medium is impossible because very large finite element meshes would need to be used. But a finite element representation of fluid medium could be used for a fully or partially submerged structure vibrating in a finite fluid medium. For example, a small dam or spill-way analysis was done by Dungar [9].

Many researchers have conducted detailed studies of the coupled finite element and boundary element method for air-structure interaction problems [26, 37, 39]. Numerical methods for modelling the fluid pressure field are usually based on boundary integral formulations, which have the advantage of reducing the dimensionality of the problem. This means that a 3-D infinite fluid medium can be modelled as a 2-D surface elements. The boundary integral equations define a relationship between the normal surface pressure and the normal surface velocity. The fluid-structure coupling is effected through matching the normal surface velocity defined in the structure to that defined by the governing equations of the fluid field. A numerical study of the air-structure interaction problem using a finite element model of the structure and the boundary element model for the air was setup by Sygulski [37], who explained how to find the natural frequency of any structure submerged in an infinite air medium. But, Sygulski [37] pointed out that the above algorithm has difficulties in finding a convergent solution for natural frequency, and several iterations have to be done to converge to a solution. The coupled finite element/boundary element analysis capability of the finite element package NASTRAN has been explained by Evertine [10, 11].

A modal study done by Fowler et al. [13] for different air pressures in a vacuum chamber on a, 3.2 m diameter and 34.7 kg, carbon graphite reflector also indicates the effect of air in the vibration analysis. The experimental results were compared with a numerical study done with the finite element package NASTRAN, which

incorporates the air mass effect. A frequency change of 12% was measured.

2.4.3 Analytical Methods

Analytical solutions for the air-structure interaction problems have been carried out by many researchers [1, 6–8, 19, 20]. An approximate solution to a coupled air-structure interaction problem can be found by using analytical methods. But the approximate solution is only possible for an infinite flat membrane lying on an infinite baffle. Therefore, this method may not be suitable for finite flat membranes.

The analytical approach to air-structure interaction are briefly reviewed as follows.

Considering a small rectangular element in a membrane under in-plane tensile force T per unit length, the following equation of motion is derived [14].

$$T\nabla^2\eta(x,y) - p(x,y) - f(x,y) = m\omega^2\eta(x,y) \tag{2.3}$$

where η is the vertical deflection of the membrane at point (x, y); p the resultant pressure acting on both sides of the membrane; f the resultant external force per unit area in the membrane and m the surface density of the membrane.

In the acoustic (fluid) medium, the steady-state fluid motion is governed by the Helmholtz equation (steady-state wave equation) as

$$(\nabla^2 + k^2)p = 0 \tag{2.4}$$

where k is the acoustic wave number.

Applying Green's theorem to Helmholtz equation (Equation 2.4) [19]

$$p = \sum \rho c V \tag{2.5}$$

where c is the sound velocity; V the fluid velocity at the boundary and ρ the density of fluid medium.

Considering velocity of the membrane and the fluid at the membrane surface

$$V(x,y) = -i\omega\eta(x,y) \tag{2.6}$$

Substituting Equations (2.6) and (2.5) into Equation (2.3), following equation is obtained

$$(\frac{T}{m\omega^2}\nabla^2\eta(x,y) - 1) = \frac{f(x,y)}{m\omega^2} + [\frac{\rho c}{m\omega}]\sum i\eta(x,y) \tag{2.7}$$

The Equation (2.7) is the fluid-structure coupling equation. The elastic problem of determining the structural response to prescribed forces, and the acoustic problem of determining the pressure in the fluid medium in response to a prescribed velocity distribution of the boundary, must be solved simultaneously. Therefore, an analytical solution to this coupled equation is impossible. However, the expression $\rho c/m\omega$ in the equation, defined as fluid loading parameter ϵ, gives an indication of the importance of considering the fluid loading mass on the vibration of a structure. Typically, for $\epsilon \ll 1$ fluid loading can be neglected.

Therefore an approximate solution to the fluid mass effect is estimated as follows [19, 20].

Considering an effectively infinite flat membrane lying on a baffle, pressure field on the boundary of the membrane is estimated by applying boundary condition to the Helmholtz equation (2.4). If the acoustic wave number k is less than structural wave number k_s, the pressure field can be expressed in terms of an inertia force of the entrained mass of fluid per unit area. The entrained mass m_a of the fluid is obtained as

$$m_a = \frac{\rho}{k_s}, \quad \text{for} \quad k_s \gg k \tag{2.8}$$

Here the entrained fluid has height of $1/k_s$ over the membrane surface. In the above derivation, fluid medium is assumed to be only on one side of the membrane. Further details to analytical solution methods are given in Chapter 6.

Chapter 3

Analysis of Membrane Structures

This chapter describes a numerical study of flat membranes and a simple membrane structure. Natural frequencies of flat membranes are from three different methods, one analytical and two computational, in section 3.1, and in section 3.2 the two different approaches are applied to the calculation of the natural frequencies of a simple membrane structure.

3.1 Flat Membranes

Three flat membrane shapes (square, triangle and L-shape) are studied focusing in particular on the variation of the fundamental natural frequency with the level of pre-tension.

The fundamental natural frequencies are calculated using three different methods: an analytical method, the Finite Element (FE) method using membrane elements and the FE method using truss elements. The accuracy of the membrane element results are checked by comparing the results with analytical and truss element results.

3.1.1 Analytical Method

The natural frequencies of a rectangular, triangular and L-shaped membrane shown in Figure 3.1 are obtained as follows.

Consider the transverse vibration of a thin and uniform rectangular flat membrane that is in equilibrium in a planar configuration, under a uniform tension T per unit length. The transverse displacement of any point on the membrane is in the direction normal to the reference surface and is assumed to be small; as a result the tension in the membrane can be assumed to be constant. Defining a

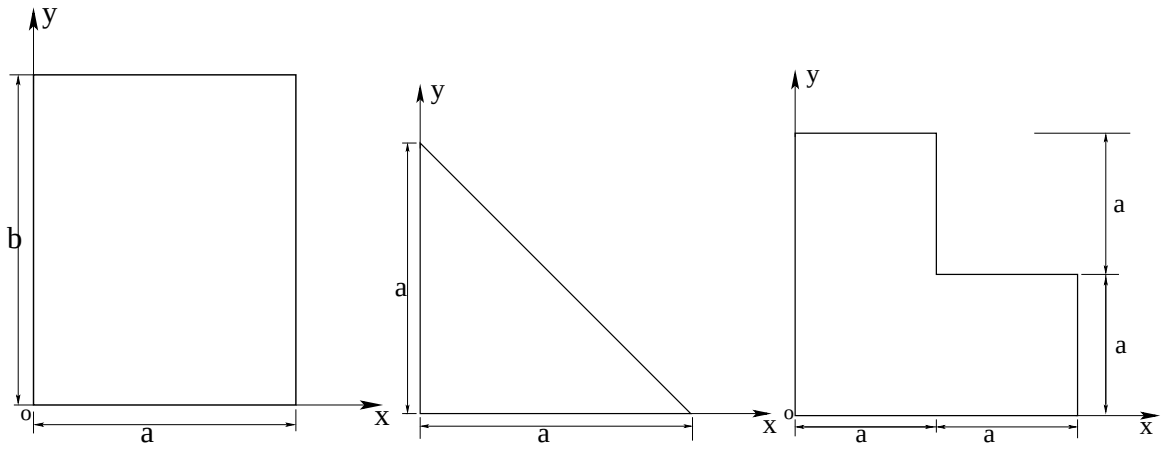

(a) Rectangle (b) Triangle (c) L-shape

Figure 3.1: Flat membranes.

coordinate system o, x, y with origin o at a corner and axes parallel to the sides of the rectangle shown in Figure 3.1(a), the governing equation of transverse motion can be written as follows [14,31];

$$T(\frac{\partial^2 \eta}{\partial x^2} + \frac{\partial^2 \eta}{\partial y^2}) = M\frac{\partial^2 \eta}{\partial t^2} \tag{3.1}$$

where η is the transverse displacement of the membrane at point (x, y), T is the uniform surface tension per unit length and M is the mass per unit area of the membrane.

For steady-state vibration at frequency ω, the transverse displacement at a point (x, y) at time t can be specified as,

$$\eta_{(x,y,t)} = \eta_{(x,y)} \cos \omega t \tag{3.2}$$

For a simply supported rectangular membrane η=0 along the boundaries, hence the mode shape is sinusoidal in both directions. Therefore, the transverse displacement η at a point (x, y) has the expression

$$\eta_{(x,y,t)} = \sin \frac{m\pi x}{a} \sin \frac{n\pi y}{b} \cos \omega t \tag{3.3}$$

Substituting Equation (3.3) into Equation (3.1) and solving for the natural frequency of vibration ω, we obtain

$$\omega_{mn} = \pi c \sqrt{\frac{m^2}{a^2} + \frac{n^2}{b^2}} \tag{3.4}$$

where m, n are integers, c the wave propagation velocity in the membrane, and c is defined as

$$c = \sqrt{\frac{T}{M}} \tag{3.5}$$

Similarly, the analytical expression for the natural frequency of a right-angled triangular membrane shown in Figure 3.1(b) is as follows [1]

$$\omega_{mn} = \pi c \sqrt{\frac{m^2 + n^2}{2A}} \tag{3.6}$$

where A is area of the triangular membrane.

An L-shaped membrane shown in Figure 3.1(c) has following expression for the fundamental natural frequency [1]

$$\omega_1 \approx \pi c \frac{1.717}{\sqrt{A}} \tag{3.7}$$

where A is area of the L-shaped membrane.

3.1.2 FE Analysis with Membrane Elements

The formulation of an analytical model for a structure having complex geometry can be extremely difficult, although it was straightforward for the rectangular flat membrane described in the previous section. The finite element (FE) method overcomes these difficulties. A detailed explanation of the FE method in structural dynamics can be obtained from references [2, 3, 5].

Flat membranes of three different shapes (square, triangular and L-shaped) were analysed using the FE package ABAQUS [17]. The square membrane has a side length of 0.2 m and a thickness of 0.1 mm; it is supported on knife edges, which act as simple supports along all four edges. Only one quarter of the membrane is considered, as shown in Figure 3.2, since the membrane is symmetrical.

The triangular membrane has base length of 0.2 m and height of 0.2 m; it is supported on knife edges along all three edges, see Figure 3.3(a). The L-shaped membrane (base length of 0.2 m) is also supported on knife edges along all six edges, see Figure 3.3(b).

The membrane is modelled using two different elements available in ABAQUS: the M3D4 membrane element which is a 4 node quadrilateral element, and the M3D3 membrane element which is a 3 node triangular element. Both are plane stress

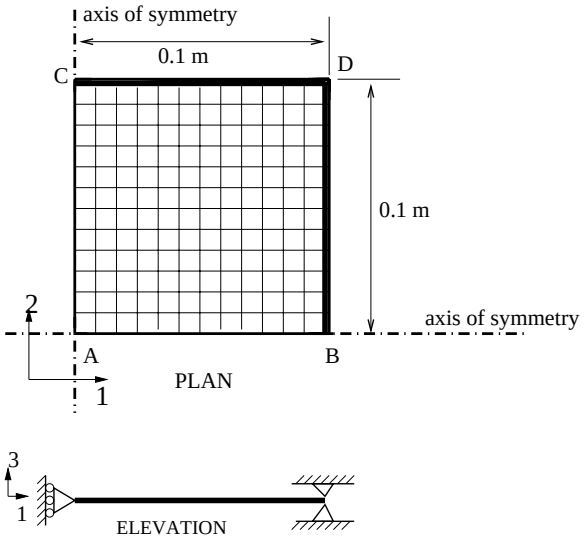

Figure 3.2: Quarter portion of square membrane.

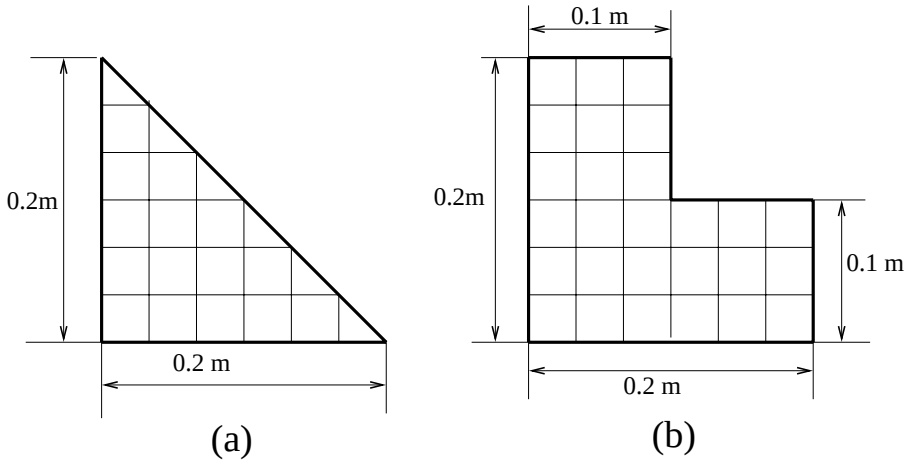

Figure 3.3: Triangular and L-shaped membranes.

elements. These elements are surface elements that transmit in-plane forces only (no moments) and have no bending stiffness. This means that it is necessary to prestress these elements before any vibration analysis is carried out. The material is assumed to be Kevlar-reinforced Kapton foil whose properties are tabulated in Table 3.1.

The mesh for the square membrane shown schematically in Figure 3.2 consists of square elements. Note that the number of elements will be kept at 100, as only a small variation in frequency was observed when the number of elements was increased to 1600, which—of course—requires much higher computation times. The following boundary conditions are applied: the nodes along the edges CD and BD are restrained in the 3-direction (vertical direction) to simulate simple supports, the nodes along the edge AB are restrained in the 2-direction because

of symmetry and similarly the nodes along the edge AC are restrained in the 1-direction. All other nodes have three degrees of freedom.

Uniform biaxial prestress is applied to the membrane elements directly using the **INITIAL CONDITIONS, TYPE=STRESS* option. This option is used before applying any of the **STEP* options. To account for the geometric stiffness induced by the prestress, non-linear calculation procedures are used. Hence, before the eigenvalue extraction calculations a non-linear static analysis step is carried out by using the **STEP, NLGEOM* option after the **INITIAL CONDITIONS* option. In the above static analysis step, the applied initial prestress is maintained by initially restraining the outer edges of the membrane. Then, in the next step (frequency extraction step), the boundary conditions are changed to the actual ones, described above, by using **BOUNDARY, OP=NEW* option.

The frequency analysis step is a linear step, therefore the non-linear option is not used here. In this option, the user can request the number of eigenvalues to be extracted, and the choice of eigensolver. There are two solution methods available in ABAQUS: the subspace iteration method and the Lanczos method. The Lanczos eigensolver is faster and more effective for models with many degrees of freedom [17, 29] and therefore it was chosen. A sample ABAQUS script is included in the Appendix A.

3.1.3 FE Analysis using Truss Elements

This analysis is performed to test the accuracy of the membrane element results, because in the case of complex membrane structures there is no reliable analytical estimate. The idea is to calibrate the truss model using flat membranes, so that it can be used to produce independent estimates later on.

The equivalent truss model for static problems was initially implemented by Hrennikoff [18] and later used by Phaal [30] to analyse shell structures. The basic idea of the method consists in replacing a continuous elastic body by a truss of pin-jointed bars, arranged according to a definite pattern, whose elements are endowed with elastic properties suitable to the type of problem; in analysing the framework and in spreading the bar stresses over tributary areas in order to obtain the stresses in the original solid body. The framework so formed is given the same external outline and boundary restraints, and is subjected to the same loads as the solid body. Hrennikoff [18], has developed this analogy for elastic problems, but the equivalence of density was not discussed in his paper. In the present study the density of the truss model is important for the frequency analysis. This problem is solved by considering the volume of material in a membrane panel and in the corresponding equivalent truss model. In this analysis, it is important to check that the total mass of the two models are equal.

The equivalent truss model set up by Hrennikoff is based on the doubly-braced

square framework shown in Figure 3.4(b), it has the same properties in both directions of the axes and has two characteristic cross-sectional areas A and A_1. Consider a membrane of Young's Modulus E, Poisson's ratio ν, thickness t and density ρ.

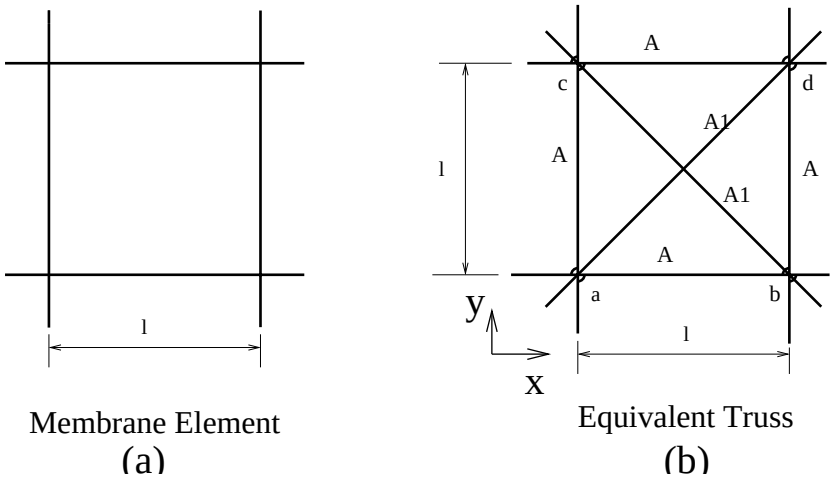

Figure 3.4: Equivalent truss model.

The values of A and A_1 can be derived as follows [18];

$$A = \frac{3}{4}lt \tag{3.8}$$

$$A_1 = \frac{3}{4\sqrt{2}}lt \tag{3.9}$$

where t is thickness of the membrane. In the derivation E and ν are assumed to be same for both membrane element and equivalent truss.

Density of the truss model (ρ_t) is estimated by equating equivalent masses of the membrane element and the equivalent truss model as

$$\rho_t = \frac{1}{3}\rho \tag{3.10}$$

Table 3.1: Properties of membrane and equivalent truss model.

Parameter	Membrane	Truss
Density (kg/m^3)	790	263
Young's Modulus (GPa)	11.9	11.9
Poisson's Ratio	0.3	0.3
Thickness (mm)	0.1	—

The equivalent truss shown in Figure 3.5 is modelled using the 3-D truss elements (T3D2) available in ABAQUS. The biaxial prestress of 10 N/m is applied in the horizontal and vertical directions, i.e. 0.05 N in each horizontal bars, 0.035 N in each diagonal bars and 0.05 N in each vertical bars, using initial conditions and similar procedures are followed as explained in the description of the membrane element.

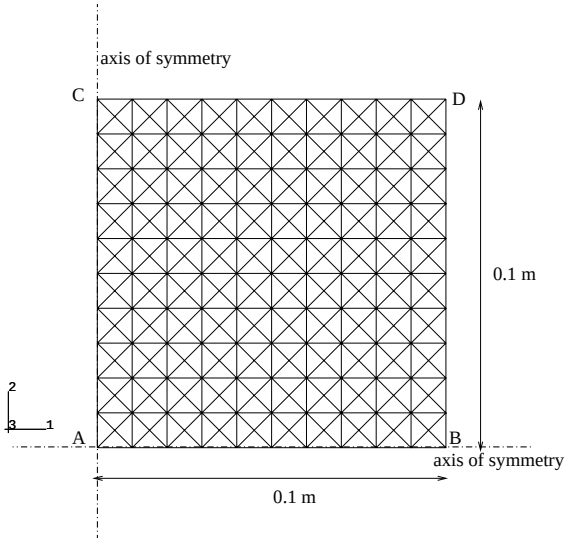

Figure 3.5: Equivalent truss model for square membrane.

3.1.4 Results

The fundamental natural frequency of the square membrane has been calculated for prestress of 10, 20, 30, 40 and 50 N/m using ABAQUS, for 100 element and 1600 element models. The truss model shown in Figure 3.5 has also been analysed. The results are tabulated in Table 3.2.

Table 3.2: Estimates of fundamental natural frequency of square membrane.

Prestress (N/m)	FE Membrane (Hz)		FE Truss (Hz)	Analytical (Hz)
	100 Elements	1600 Elements		
10	39.66	39.76	39.73	39.78
20	56.08	56.23	56.19	56.25
30	68.69	68.87	68.81	68.90
40	79.31	79.52	79.46	79.56
50	88.67	88.90	88.84	88.95

The fundamental natural frequencies of the triangular and L-shaped membrane with prestress of 10 N/m have also been calculated with ABAQUS and with Equations (3.6) and (3.7). Their values are tabulated in Table 3.3.

Table 3.3: Estimates of fundamental natural frequency of various membranes.

Model	FE (Hz)	Analytical (Hz)
Square	39.66	39.78
Triangle	61.60	62.90
L-shape	55.44	55.77

3.2 Simple Membrane Structure

The structure shown in Figure 3.6 consists of two main parts: four 1 m long vertical ribs fixed at the bottom, and a thin membrane square tube that is supported and tensioned by the ribs. The ribs have circular cross-section of 2 mm radius; the membrane has a thickness of 0.1 mm and each panels is 0.5 m wide. The membrane is prestressed by applying a biaxial tension of 100 N/m in the horizontal and the vertical directions before the frequency analysis is carried out.

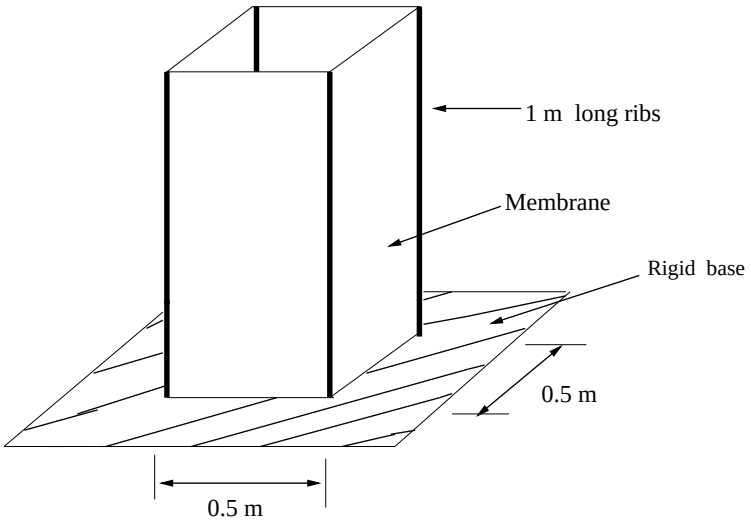

Figure 3.6: Simple membrane structure.

The natural frequencies of this structure were compared with two different approaches, to check the accuracy of the membrane element calculations in ABAQUS. First, the membrane panels are modelled using membrane elements; second, the equivalent truss model is used.

3.2.1 FE Analysis

The ribs are modelled with $B33$ beam elements. These are Euler-Bernoulli beam elements, which do not allow for transverse shear deformation, based on cubic interpolation functions which make them reasonably accurate for cases involving

distributed loading along the beam. Therefore they are well suited for dynamic vibration analysis. Steel material properties are assigned to the ribs, as shown in Table 3.4. The membrane is modelled using the four node membrane elements (M3D4) described in section 3.1.2. Material properties of the membrane are specified in Table 3.4.

Table 3.4: Properties of ribs and membrane.

Parameter	Rib	Membrane
Density (kg/m^3)	7000	1
Young's Modulus (GPa)	200	20
Poisson's Ratio	0.3	0.3

The biaxial prestress of 100 N/m is applied to the membrane in all four faces of the structure as explained in Section 3.1.2. When the prestress is applied, it is kept in the membrane panels by fixing their all four edges. Therefore, the prestress is preserved in the membrane panels before the frequency analysis is carried out. In the frequency analysis step, previously fixed edges are released and actual boundary conditions are applied.

The analysis was repeated using a truss element model shown in Figure 3.7. The model consists of 3-D truss elements (T3D2) with an initial biaxial prestress of 100 N/m in the horizontal and the vertical directions, i.e. 5 N in each horizontal bars, 3.54 N in each diagonal bars and 5 N in each vertical bars.

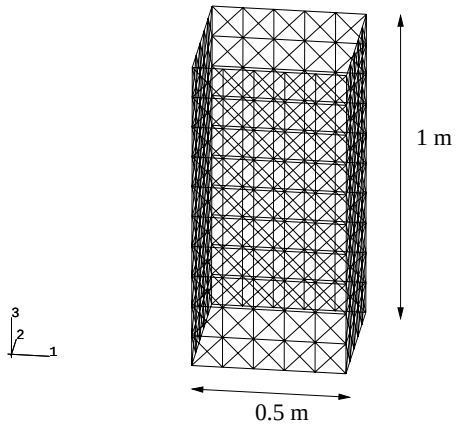

Figure 3.7: Equivalent truss model.

3.2.2 Results

Table 3.5 lists the natural frequencies obtained from the two methods, for biaxial prestress of 100 N/m.

The first four mode shapes of the membrane structure are plotted in Figures 3.8 and 3.9.

Table 3.5: Natural frequencies of simple structure.

Modes	Natural Frequency (Hz)	
	Membrane Model	Truss Model
1	289.54	288.04
2	309.80	309.51
3	309.83	309.51
4	333.11	334.42
5	804.18	785.12
6	828.95	826.84
7	828.95	826.84
8	828.95	829.59
9	828.95	829.59

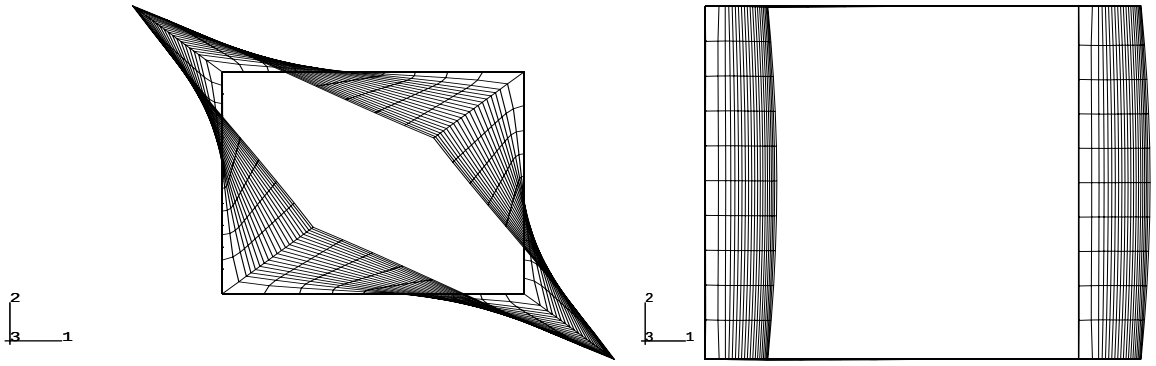

(a) Mode 1 (289.54 Hz)

(b) Mode 2 (309.80 Hz)

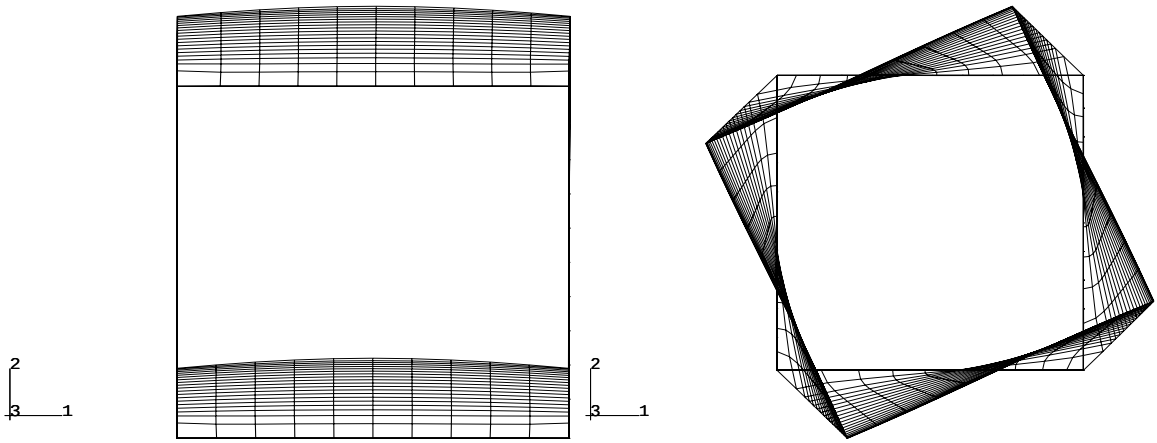

(c) Mode 3 (309.83 Hz)

(d) Mode 4 (333.11 Hz)

Figure 3.8: Top views of first four mode shapes.

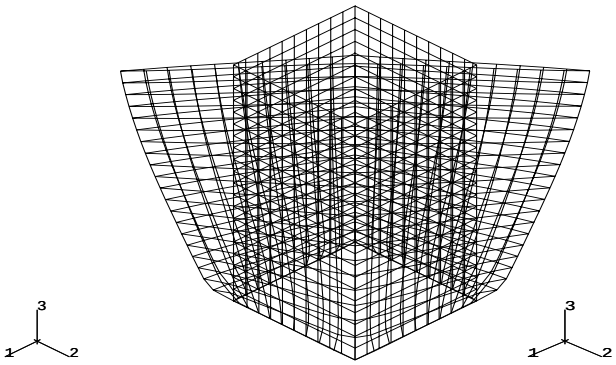

(a) Mode 1 (289.54 Hz)

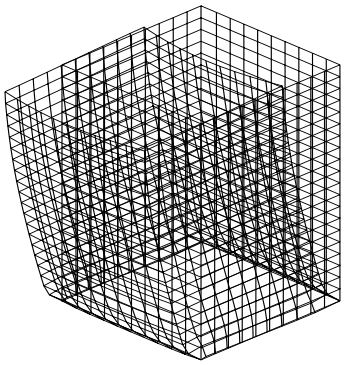

(b) Mode 2 (309.80 Hz)

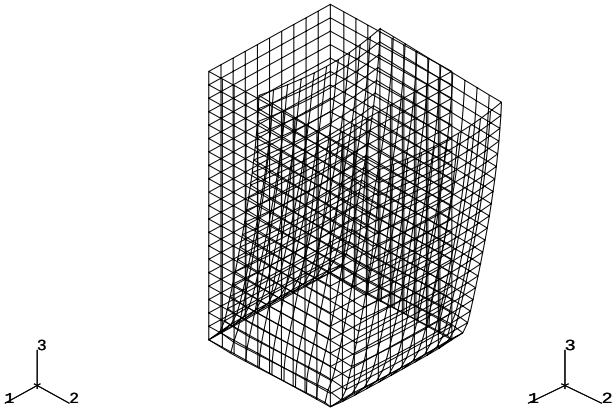

(c) Mode 3 (309.83 Hz)

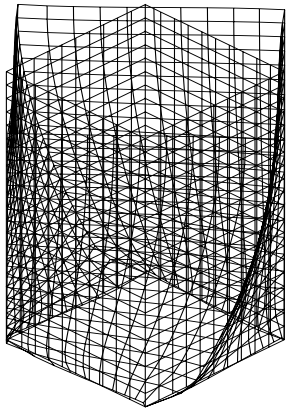

(d) Mode 4 (333.11 Hz)

Figure 3.9: Isometric views of first four mode shapes.

3.3 Discussion

For the flat membrane results, note—Table 3.2—that the finite element results from the membrane model with different mesh modelling show only a very small difference in frequency, although the fine mesh requires a large amount of computation. Therefore, these results encourage the use of moderately coarse meshes in further work.

The three sets of results in Table 3.2 show good agreement between finite element and analytical solutions. This suggests ABAQUS can be used reliably to estimate natural frequencies using four node membrane elements (M3D4). It can also be concluded that the truss model based on element T3D2 is broadly in agreement

with the other analyses. Finally, Table 3.2 shows how the fundamental natural frequency of the membrane increases with the applied prestress; this is because the geometric stiffness of the membrane increases with the prestress level.

Similar observation can be made for Table 3.3, for the triangular and L-shaped membrane. From these studies, it is clear that the membrane element (M3D4) in ABAQUS can be used to analyse any shape of membrane models.

For the simple membrane structure model analysed in section 3.2 it is observed in Table 3.5, that the membrane model and the truss model give similar results, with the exception of the fifth mode. The results indicate that the membrane elements in ABAQUS can confidently be used for analysis of any membrane structures.

Chapter 4

Analysis of CRTS Reflectors

This chapter presents a study of the natural frequencies of a deployable membrane reflector antenna in the deployed configuration. The effects of changing the diameter, hub radius and membrane prestress on the fundamental natural frequency are studied using ABAQUS. Results are presented for 1.5, 5 and 10 m diameter reflectors with 6, 12 and 24 ribs. Section 4.1 gives a brief introduction to the reflector. Modelling and analysis of the reflector using ABAQUS are explained in section 4.2. Section 4.3 presents the results that have been obtained; a comparison between membrane and truss element models is conducted. Section 4.4 discusses the results in the section 4.3.

4.1 Introduction

The CRTS reflector is a new generation of large space reflectors that is being developed by the European Space Agency [32]. Its equilibrium shape and shape accuracy have been extensively studied in the Deployable Structures Laboratory, University of Cambridge [22–24]. The CRTS reflector consists of three main parts: a central expandable hub, a series of thin-wall foldable ribs connected radially to the hub and a precision-shaped membrane that is supported and tensioned by the ribs.

The CRTS reflector is generally lightweight and relatively flexible, and there is the possibility that vibration of the reflector in the deployed configuration, induced by the attitude control system of the spacecraft may degrade its intended performance. The dynamic response of a structure is mainly dependent on the coupling between dynamic loads exerted on the structure and the dynamic characteristics of the structure itself. If the frequency of the exciter is close to one of the natural frequencies of a structure, the maximum response of the structure will be induced. Therefore in the design of large deployable appendages it is customary to change the mass and stiffness distribution of the appendage to

move the natural frequencies away from the rigid-body frequencies of the spacecraft. This approach is widely used in the dynamic design of reflector structures and therefore, knowledge of the natural frequencies of the CRTS reflector is an important problem in the dynamic design of the reflector.

A special feature of symmetric CRTS reflectors (not those with offset configuration) is their periodic nature. A symmetric reflector consists of a number of identical repetitive units, or substructures. Therefore the analysis of the reflector can be simplified considerably by considering its periodic nature [33,34]. But in the actual model perfect periodicity cannot be expected. Therefore, even small imperfections in the model can cause the predictions of the natural frequency and mode shapes to be completely incorrect [4]. Although this is not the scope of this dissertation, it is clear that an experimental analysis will have to be carried out later on.

Returning to the vibration problem, it is impossible to obtain analytical (exact) solutions of the reflector. Therefore, finite element (approximate) solutions will be used. The accuracy of which will be assessed by modelling the reflector using both membrane elements (M3D4) and truss elements (T3D2) in the ABAQUS simulations, and by comparing the results.

4.2 Modelling and Analysis

The shape of the reflector is assumed to be a paraboloid, whose equation is given by

$$Z = \frac{X^2 + Y^2}{4F} \tag{4.1}$$

where Z is the height above the $X - Y$ plane, and the X, Y the Cartesian co-ordinates are measured from the centre of the reflector. F is the focal length, D the diameter. The European Space Agency is currently considering reflector with

$$\frac{F}{D} = 0.78 \tag{4.2}$$

Therefore this ratio type of reflectors are considered in this dissertation. The membrane of the reflector is Kevlar-reinforced Kapton foil and the ribs are made of Copper-beryllium. Their material properties are given in Table 4.1.

Several different configurations of the reflector are considered: 6, 12, 24 ribs, and 1.5, 5 and 10 m diameters. The membrane is assumed to be singly-curved between each set of two ribs.

The nodal coordinates of a gore were defined using a MATLAB program. These nodes define a set of triangular elements. The nodal co-ordinates of the remaining gores were created using the **NCOPY, SHIFT, MULTIPLE="no. of gore"*

Table 4.1: Material properties of ribs and membrane.

Parameter	Ribs	Membrane
Density (kg/m^3)	8400	790
Young's Modulus (GPa)	131	11.9
Poisson's Ratio	0.3	0.3
Thickness (mm)	0.2	0.1

option available in ABAQUS. After defining the element numbers in the first gore, the element numbers of the remaining gore were simply created using the ABAQUS option **ELCOPY, OLD SET=() , SHIFT NODE=() , ELEMENT SHIFT=() , NEW SET=()*. The default local axis direction of each gore is parallel to the global axis, but it is necessary to define a local axis parallel to the base of each gore because the stress in each element is defined in the local axis. The initial prestress in the membrane, in each gore is applied, parallel to the base, in the 1-local axis direction using the option **INITIAL CONDITIONS, TYPE=STRESS*. Along the ribs two sets of coinciding nodes are defined, and in each gore; these nodes are tied together using the option **MPC* .

The triangular membrane elements are modelled using M3D3 membrane elements. An initial uniaxial prestress of 100 N/m is applied in the local 1-direction in each gore. In the dummy static analysis step, the nodes along the ribs are restrained. Then, in the frequency analysis step, the boundary conditions are released, and the rib connecting nodes in the base are restrained using **BOUNDARY, OP=NEW* option.

The ribs are modelled with B33 beam elements. The ribs have open-section with 0.2 mm thickness; their cross-section is shown in Figure 4.1. The cross-section of the rib is specified using the option **BEAM SECTION, SECTION=ARBITARY*, and the 5 points of the cross-section are specified in the next line, in ABAQUS. Figure 4.1 shows the actual cross-section of the rib, and the approximated cross-section. The orientation of the beam cross-section is defined in terms of a local, right handed, axis system. This is achieved by defining the approximate rib direction in the option **BEAM SECTION*.

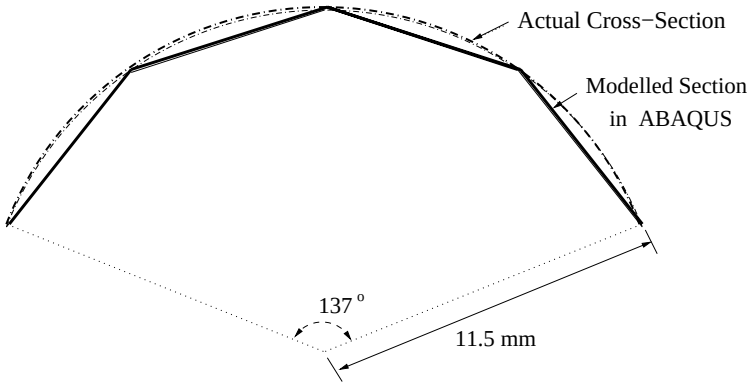

Figure 4.1: Actual and modelled shape of rib cross-section.

The finite element model of a 1.5 m diameter reflector with 12 ribs is shown in Figure 4.2.

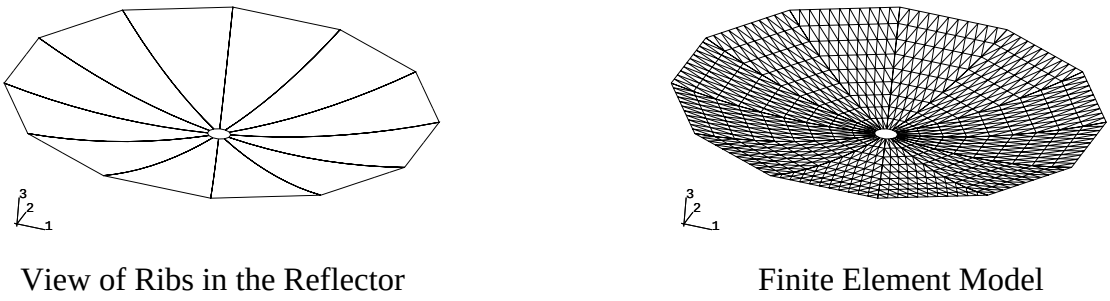

Figure 4.2: Model of 1.5 m diameter reflector with 12 ribs.

The frequency analysis was also done with prestress of 50 N/m and 200 N/m, for the 1.5 m diameter reflector. In the above analysis, a minimum value of the hub radius was used to model reflectors with different numbers of ribs. The calculation of the minimum hub radius is explained as follows. Figure 4.3 shows a top view of the hub region defining the minimum hub radius of a reflector with 6 ribs.

Consider triangle OAB,

$$\tan\frac{\theta}{2} = \frac{l}{2r} \tag{4.3}$$

then,

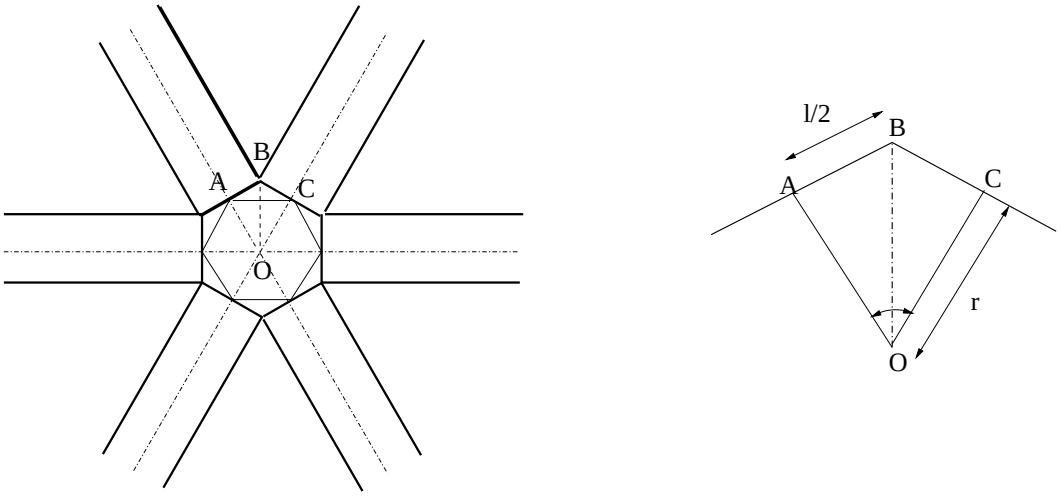

Figure 4.3: Minimum hub radius configuration.

$$r = \frac{l}{2 \tan \frac{\theta}{2}} \tag{4.4}$$

For a reflector with 6 ribs each 21.4 mm wide, Equation 4.4 gives r = 18.5 mm. Similarly for 12 ribs ($\theta = 30°$), r = 40 mm and for 24 ribs ($\theta = 15°$), r = 82 mm.

The natural frequencies of a 10 m diameter reflector were analysed for different hub radii. Detailed results are presented in the following section.

Then, the natural frequencies of the 1.5 m diameter reflector with 6 ribs, were computed using the equivalent truss model approach.

4.3 Results

4.3.1 Reflector with Small Hub

The first fifteen natural frequencies of the 1.5 m diameter reflector with three different numbers of ribs are tabulated in Table 4.2. The prestress is 100 N/m in the hoop direction. The first nine mode shapes of the reflector with 6 ribs are plotted in Figures 4.4 and 4.5.

Table 4.2: Natural frequencies of 1.5 m diameter reflectors with $F/D = 0.78$.

Mode	Frequency (Hz)		
	6 ribs	12 ribs	24 ribs
1	16.46	17.78	17.40
2	16.46	17.78	17.40
3	17.51	18.05	20.64
4	17.51	18.05	20.64
5	22.16	27.93	29.22
6	23.57	27.93	29.22
7	23.71	37.66	41.50
8	24.61	37.66	41.50
9	24.61	39.87	41.95
10	25.04	42.11	43.95
11	25.04	42.11	43.95
12	29.78	42.13	43.97
13	31.59	42.13	43.97
14	31.59	42.13	43.98
15	34.67	42.13	43.98

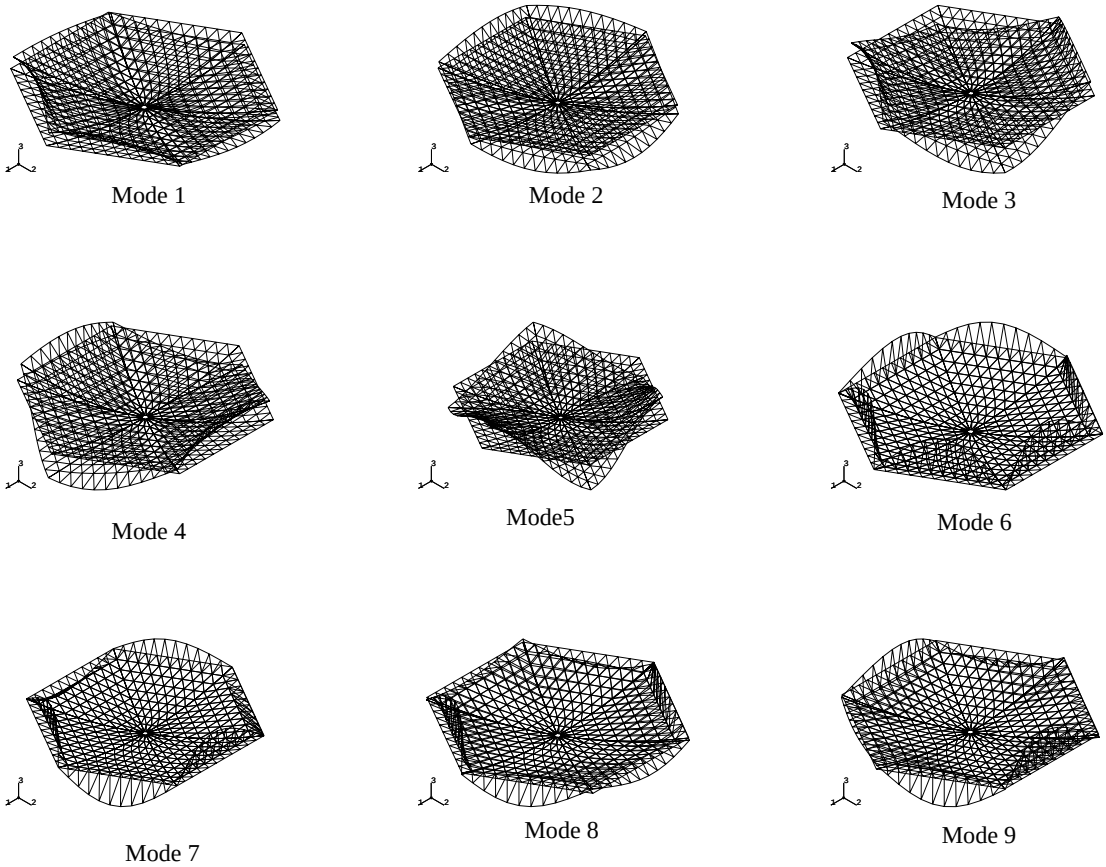

Figure 4.4: Mode shapes of 1.5 m diameter reflector with 6 ribs.

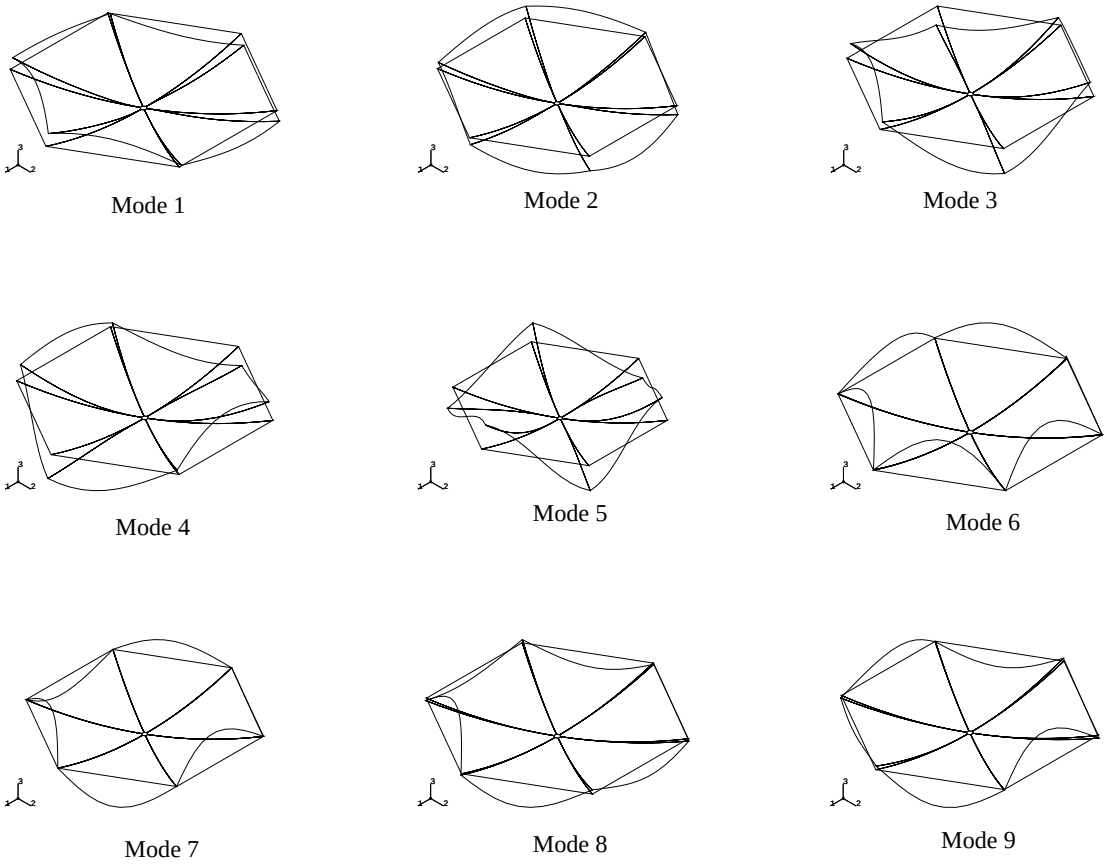

Figure 4.5: Outline of mode shapes shown in Figure 4.4.

Table 4.3 gives the first fifteen natural frequencies of a 5 m diameter reflector with three types of ribs. The first nine mode shapes of the reflector with 12 ribs are plotted in Figures 4.6 and 4.7.

Table 4.3: Natural frequency of 5 m diameter reflector with $F/D = 0.78$.

Mode	Frequency (Hz)		
	6 ribs	12 ribs	24 ribs
1	3.14	2.97	2.85
2	3.14	2.97	2.85
3	5.09	4.55	4.01
4	5.09	4.55	4.01
5	6.74	6.60	5.96
6	6.89	6.60	5.96
7	7.12	8.61	8.04
8	7.47	8.61	8.04
9	7.47	9.41	10.18
10	7.54	10.36	10.18
11	7.54	10.39	11.87
12	7.60	10.39	12.33
13	8.49	11.30	12.33
14	9.00	13.75	12.69
15	9.30	14.18	14.43

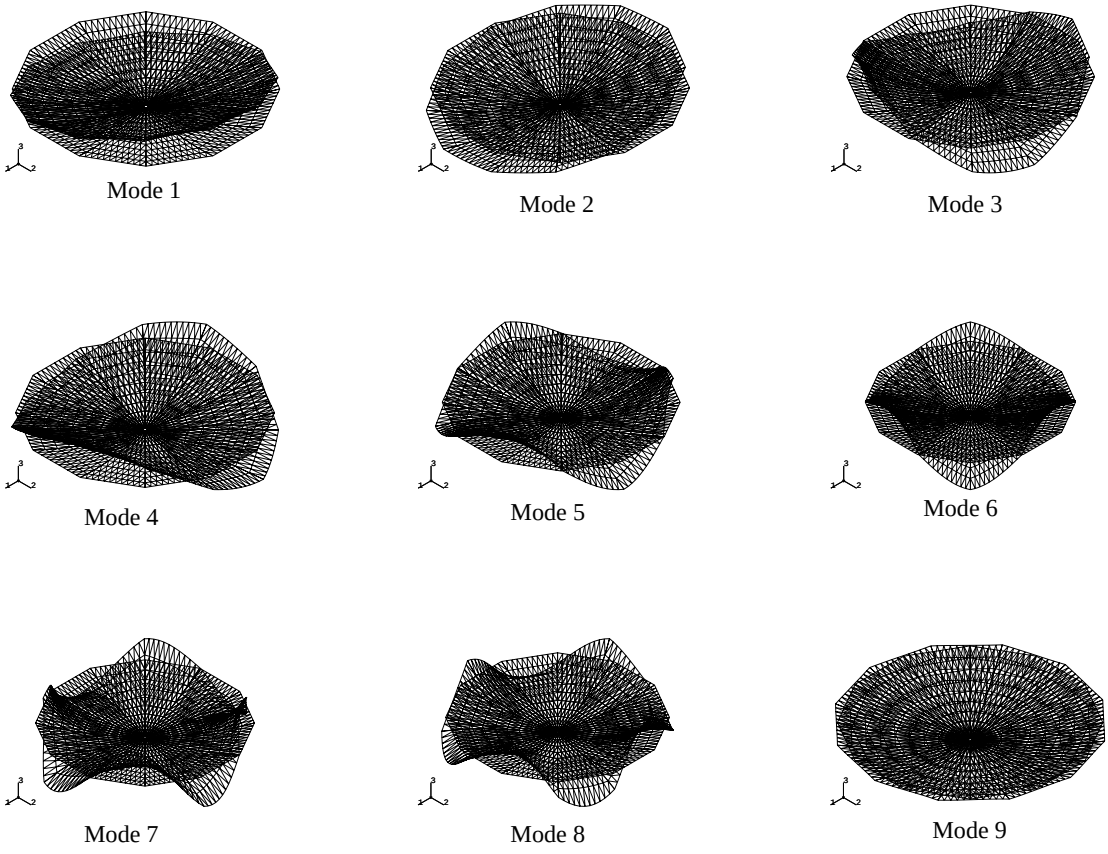

Figure 4.6: Mode shapes of 5 m diameter reflector with 12 ribs.

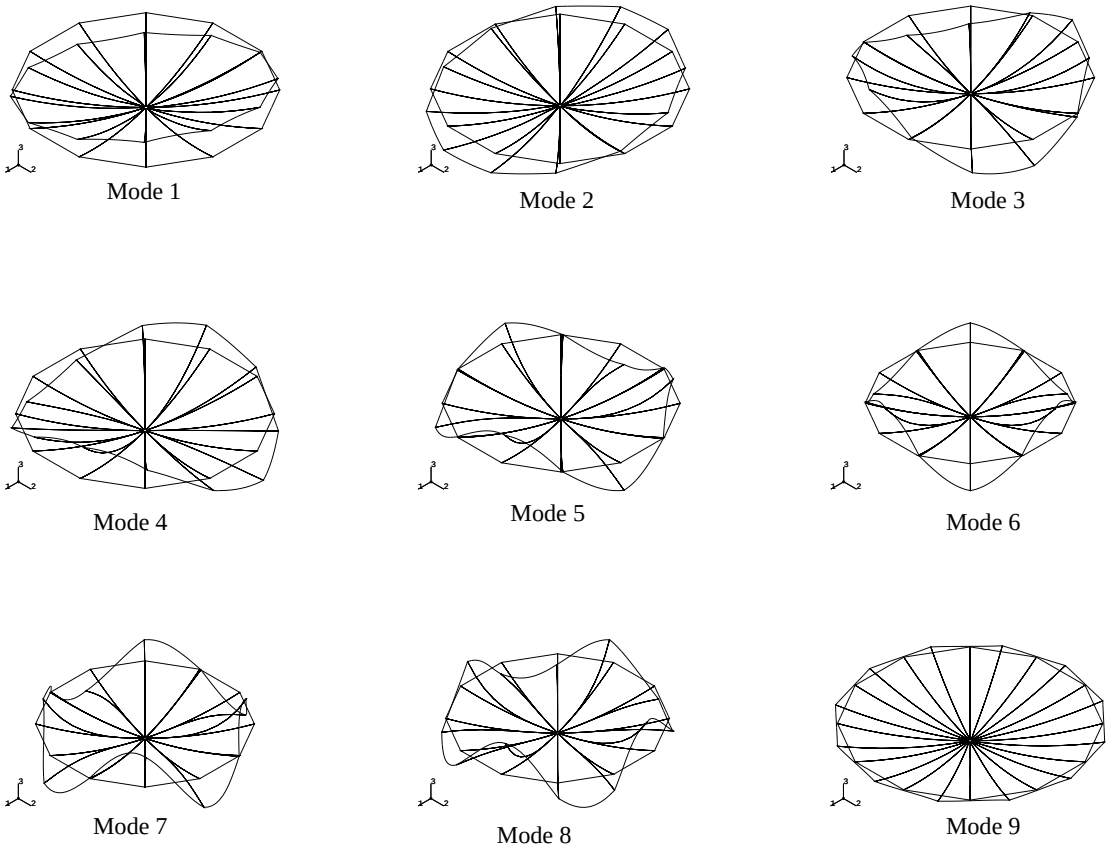

Figure 4.7: Outline of mode shapes shown in Figure 4.6.

Table 4.4 shows the first fifteen natural frequencies of a 10 m diameter reflector with different number of ribs. The first nine mode shapes for 24 ribs are plotted in Figures 4.8 and 4.9.

Table 4.4: Natural frequency of 10 m diameter reflector with $F/D = 0.78$.

Mode	Frequency (Hz)		
	6 ribs	12 ribs	24 ribs
1	1.54	1.43	1.32
2	1.54	1.43	1.32
3	2.72	2.47	2.23
4	2.72	2.47	2.23
5	2.78	3.35	3.21
6	2.93	3.48	3.21
7	3.56	3.56	3.99
8	3.74	3.56	4.21
9	3.75	4.63	4.21
10	3.75	4.63	4.57
11	3.76	5.63	5.21
12	3.84	5.63	5.21
13	3.84	6.26	6.21
14	4.52	6.87	6.21
15	4.56	6.98	7.20

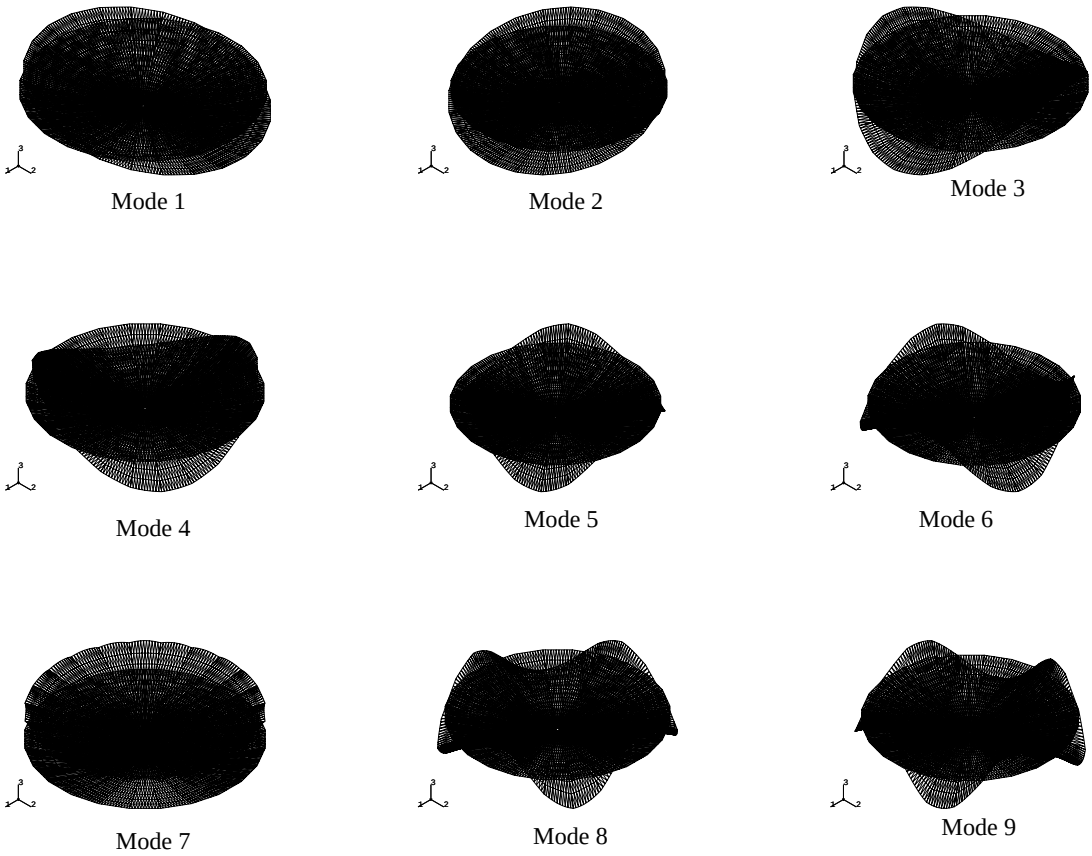

Figure 4.8: Mode shapes of 10 m diameter reflector with 24 ribs.

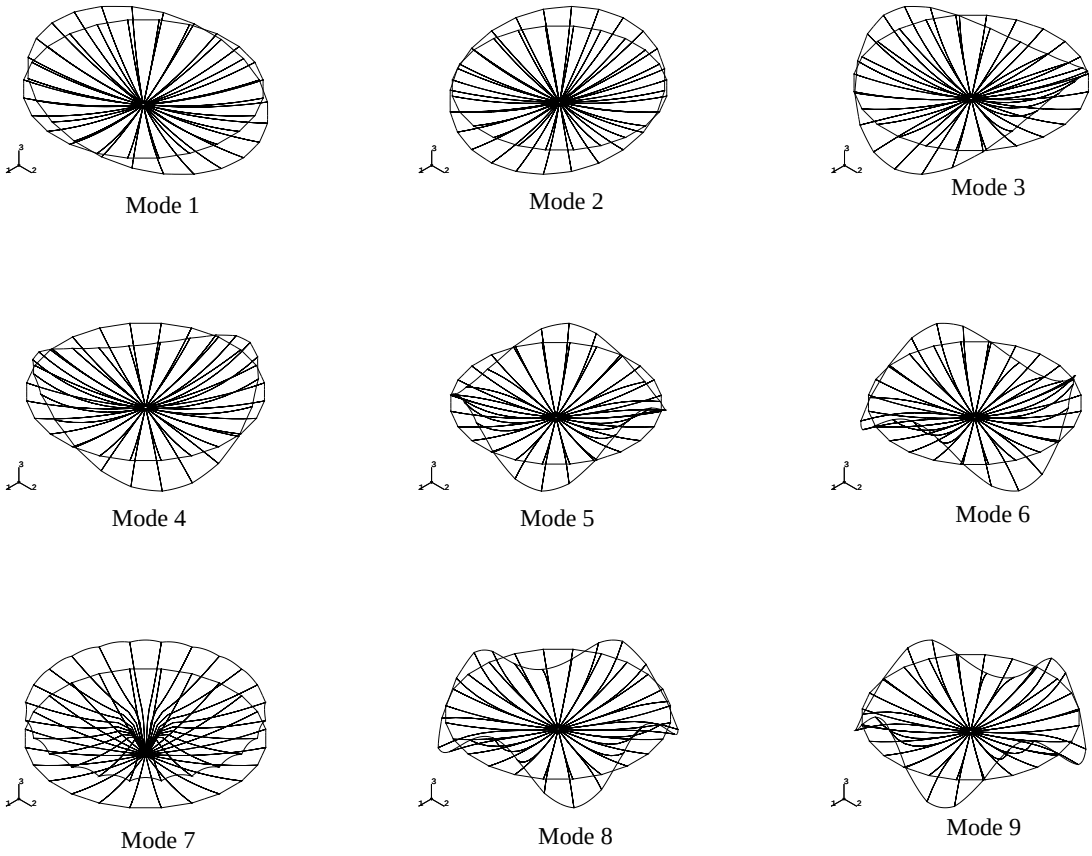

Figure 4.9: Outline of mode shapes shown in Figure 4.8.

4.3.2 10 m Reflector with Different Hubs

The first nine natural frequencies of the 10 m diameter reflector were calculated for different hub radii. Detailed results are given in Table 4.5.

Table 4.5: Natural frequencies of 10 m diameter reflector with different hub radii.

Mode	Frequency (Hz)								
	6 ribs			12 ribs			24 ribs		
	20mm	40mm	80mm	40mm	80mm	160mm	82mm	150mm	300mm
1	1.54	1.54	1.55	1.43	1.44	1.46	1.32	1.34	1.42
2	1.54	1.54	1.55	1.43	1.44	1.46	1.32	1.34	1.42
3	2.72	2.71	2.72	2.47	2.47	2.47	2.23	2.23	2.23
4	2.72	2.72	2.72	2.47	2.47	2.47	2.23	2.23	2.23
5	2.78	2.91	3.07	3.35	3.41	3.56	3.21	3.21	3.21
6	2.93	3.56	3.56	3.49	3.56	3.56	3.21	3.21	3.21
7	3.56	3.75	3.75	3.56	3.56	4.17	3.99	4.21	4.21
8	3.74	3.75	3.75	3.56	4.63	4.63	4.21	4.21	4.21
9	3.75	3.76	3.76	4.63	4.63	4.63	4.21	4.45	5.21

4.3.3 Variation of Frequency with Prestress

The natural frequencies of 1.5 m diameter reflector were calculated with prestress of 50, 100 and 200 N/m in the hoop direction. In the analysis, the minimum hub radius was used. The results are tabulated in Table 4.6.

Table 4.6: Natural frequency of 1.5 m diameter reflector with different prestress.

Mode	Frequency (Hz)								
	Stress = 50N/m			Stress = 100N/m			Stress = 200N/m		
	6 ribs	12 ribs	24 ribs	6 ribs	12 ribs	24 ribs	6 ribs	12 ribs	24 ribs
1	14.63	15.87	16.14	16.46	17.78	17.40	18.27	19.12	19.56
2	14.63	15.87	16.14	16.46	17.78	17.40	18.27	19.12	19.56
3	14.65	17.37	20.30	17.51	18.05	20.64	21.66	20.96	21.21
4	14.65	17.37	20.30	17.51	18.05	20.64	21.66	20.96	21.21
5	16.72	24.94	27.48	22.16	27.93	29.22	27.02	32.28	32.12
6	16.77	24.94	27.48	23.57	27.93	29.22	33.08	32.28	32.12
7	17.98	30.91	39.15	23.71	37.66	41.50	33.54	39.64	42.11
8	17.98	30.91	39.15	24.61	37.66	41.50	34.49	41.84	44.09
9	18.87	32.04	41.87	24.61	39.87	41.95	34.49	41.84	44.09

4.3.4 Comparison of Membrane and Truss Models

The natural frequencies of a 1.5 m diameter reflector with 6 ribs were calculated by two different approaches. In the first approach, membrane elements were used to model the membrane. In the other approach, a triangular framework of pin-jointed elements were used to model the membrane, as explained in section 3.1.3. The results are tabulated in Table 4.7.

Table 4.7: Comparison of natural frequencies of 1.5 m diameter reflector with 6 ribs.

Mode	Frequency (Hz)	
	Membrane Model	Truss Model
1	16.46	16.11
2	16.46	16.11
3	17.51	17.06
4	17.51	17.06
5	22.16	21.75
6	23.57	22.87
7	23.71	22.92
8	24.61	22.95
9	24.61	22.95

The first nine mode shapes are plotted in Figure 4.10.

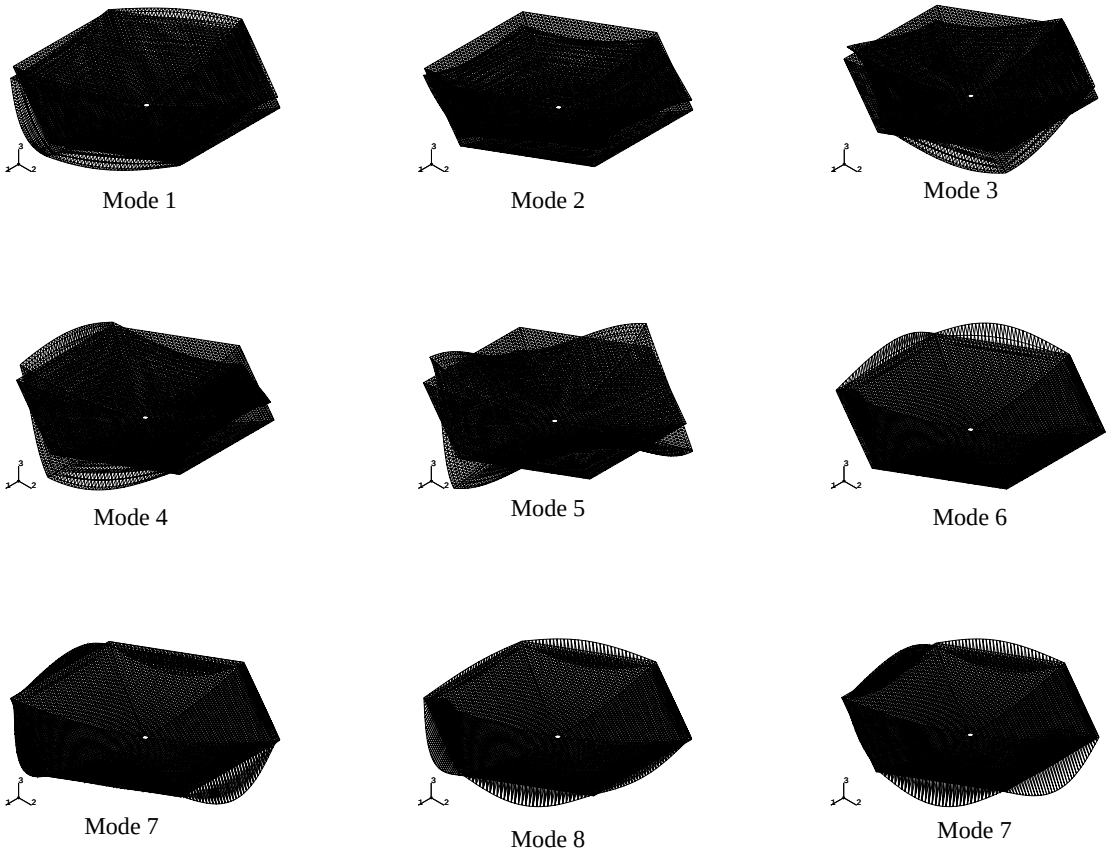

Figure 4.10: Mode shapes of 1.5 m diameter reflector with 6 ribs modelled as a framework.

4.4 Discussion

4.4.1 Reflector with Small Hub

The natural frequency variation of the 1.5 m diameter reflector with the number of ribs is shown in Table 4.2. It is observed that the frequency increases with the number of ribs, although a slight variation is seen in the first two frequencies of the reflectors with 12 and 24 ribs.

Table 4.3 gives the natural frequencies of 5 m diameter reflector with different number of ribs. The frequency decreases with the increased number of ribs, but a variation to this pattern is observed for the last three modes. The same behaviour is observed—Table 4.4—for the 10 m diameter reflector, but only for the first four

modes. But in this reflector, a complex variation is observed in the remaining modes.

The natural frequency of a structure depends on its stiffness and mass. When the number of ribs is changed, both the stiffness and the mass of the reflector change. This explains why the behaviour observed in the above results does not show a single trend. It should also be noticed that in increasing the number of ribs no attempt has been made to optimise the design of the structure, e.g. by decreasing the cross-section of the ribs or increasing the level of prestress.

As expected, from the three tables, it is observed that the natural frequencies of the reflector decrease with the increment of its diameter. When the diameter of the reflector is increased, the stiffness of the reflector decreases but the mass of the reflector increases. This explains the reason for the decreasing natural frequency with increment in the diameter.

In all three tables, one important common feature can be observed that two different modes exist at a given natural frequency. It can also be seen that the number of ribs used in the reflector is equal to the number of normal modes observed in a group, e.g. 6 ribs reflector has 6 normal modes in a group and 12 ribs reflector has 12 normal modes in a group, although the number of natural frequencies in a group is less than the number of ribs. Therefore this observation confirms that the number of normal modes in a given propagation zone is equal to the number of substructures or identical repetitive units. This observation agrees with the observation made by SenGupta [34], as explained in section 2.3. This clearly shows the periodic nature of the reflector.

4.4.2 10 m Reflector with Different Hubs

Table 4.5 gives the natural frequencies of the 10 m diameter reflector with various hub radii. One important point that is observed from the table is that the frequency does not change greatly with the hub radius, although in a very few cases it is not. Overall, a small increase in frequency is observed when the hub radius is increased.

A periodic pattern is observed in the frequencies as discussed in the previous section. In addition, it is observed that the periodicity of the reflector is preserved with increase of the hub radius.

It can be concluded that the hub radius does not have a major effect on the natural frequency of the reflector and the periodicity of the reflector.

4.4.3 Variation of Frequency with Prestress

Table 4.6 shows the natural frequencies of 1.5 m diameter reflectors with initial stress of 50, 100, 200 N/m. As expected, the frequency increases with the increase of prestress. The increase of frequency is less in the lower modes than in the higher modes.

As discussed in previous sections, the existence of two different modes at a given natural frequency is observed. This observation also ensures the periodic nature of the reflector.

4.4.4 Comparison of Membrane and Truss Models

Table 4.7 shows the natural frequencies of 1.5 m diameter reflectors (6 ribs) with membrane and framework elements. Similar results are observed from both types of analysis, which is reassuring. This confirms the accuracy of the membrane model. The periodic pattern is observed in the truss model results as well.

Chapter 5

Experiments on Flat Membrane

This chapter describes the experiments undertaken on a flat membrane. Section 5.1 gives a brief introduction to the analysis of the experimental results. The experimental set-up for the impulse excitation and the slow sine sweep method is explained in section 5.2. Experimental and numerical results are presented and discussed in section 5.3.

5.1 Introduction

Experiments have been undertaken to find the natural frequency and mode shape of a three-sided flat membrane. The membrane was a single sheet of Mylar with inwardly curved edges tensioned by thin Kevlar cables encased in the edges.

The natural frequency of the membrane was calculated using a digital vibration analysis procedure. The membrane was excited by impulses applied to a turnbuckle at the corner of the membrane and the output was measured using a laser vibrometer. In this experiment, both excitation (input) and response (output) signals were measured. A series of repeated measurements were made under nominally identical conditions and then the power spectrum and the cross spectrum were averaged before computing the frequency response and coherence functions. This method is called *averaging*. Further explanation of the above method can be found in references [12, 16, 36].

The Frequency Response Function (FRF) of a single input-output system is defined as the ratio of the Fourier transforms of the response (output) to the excitation (input)

$$\text{FRF} = \frac{V(f)}{U(f)} \tag{5.1}$$

where $V(f)$ is the Fourier transform of the system output and $U(f)$ is the Fourier transform of the system input.

In this equation, the measured frequency response will be a good approximation to the true frequency response only if the measurement noise at both the input and output measurement points is small relative to the input and output signals. Therefore, in practice, the frequency response functions are calculated by computing the ratio of the cross-spectrum between input and output to the power spectrum of the input

$$\text{FRF} = \frac{G_{uv}(f)}{G_u(f)} \tag{5.2}$$

where $G_{uv}(f)$ is the cross-spectrum between input and output signals and $G_u(f)$ is the power spectrum of the input.

This relationship is derived by multiplying the numerator and denominator of the right hand side of the Equation (5.1) by the complex conjugate of the input Fourier transform. If the noise to signal ratio at the input measurement point is significantly less, the measured frequency response will closely approximate the true FRF. There is an inherent bias error associated with the computation of the cross spectrum and the magnitude of this bias error is inversely proportional to the number of averages used in the computation. Thus, the greater the measurement noise, the greater the number of averages required to approach the expected value of the cross-spectrum between the input and the output measurement signals. Anyhow, the bias error cannot be reduced significantly by taking many averages so that it is necessary to minimise the noise in the measurement of the input signal [15].

The coherence function between input and output signals is defined by Equation 5.3. The coherence function will be identically equal to 1 if there is no measurement noise and the system is linear. The minimum value of the coherence function is 0, which occurs when the two signals are totally uncorrelated. Therefore, the coherence function is a measure of the two signals in terms of noise and nonlinear effects.

$$\text{Coherence} = \frac{|G_{uv}(f)|^2}{G_u(f)G_v(f)} \tag{5.3}$$

Impulse technique applications and problems associated with them are clearly outlined in Halvorsen and Brown [16]. The procedure for finding the natural frequency is explained in the following section.

The mode shapes and natural frequencies of the membrane were obtained by the slow sine sweep method using a loudspeaker arrangement. Although this experiment was not fully successful in finding the mode shapes, the natural frequencies

were obtained. This is also explained in the following section.

A numerical analysis of the above model was done using ABAQUS. Finite element meshes of the model were generated using PATRAN [25] and analysed in ABAQUS. The three sets of results obtained from these different methods are compared in section 5.3. A large difference between experimental and numerical natural frequencies is observed which indicates the effect of air on the vibration of the model. This effect will be further discussed in Chapter 6.

5.2 Experimental Set-up

5.2.1 Test Specimen

The geometrical features of the three-sided flat membrane are shown in Figure 5.1 and the material properties are given in Table 5.1. Along each edge of a right angle triangle, there is a cord forming a circular arc with sag to depth ratio of 20. The membrane is 0.1 mm thick Mylar; the Kevlar cables of 0.92 mm diameter are attached to all three edges with Kapton tape. The pair of cables that meet at a corner are glued to form a single cable which is fixed to a bracket through a turn-buckle. The turn-buckles are arranged to meet at a point as indicated in the figure, for equilibrium. A strain gauge is attached to one cable, as shown in the figure, and the required tension in the membrane is achieved by adjusting the turn-buckles manually while carefully monitoring the calibrated strain-gauge reading with a Wheaston circuit meter. The experiment was conducted for a stress value of 20 N/m in the membrane which was achieved by adjusting the turn-buckles until a reading of 29.6 N was obtained in the strain-gauge.

Table 5.1: Material properties of membrane and cable.

Parameter	Membrane	Cable
Density (kg/m^3)	1390	1450
Young's Modulus (GPa)	11.9	131
Poisson's Ratio	0.3	0.3

5.2.2 Natural Frequencies

The membrane model was excited by impulse excitation method. This method consists in applying a small impact on one of the turn-buckles with a small hammer while a Ploytec OFV 302 laser vibrometer was focused on a target point on the membrane surface. The input force signals were detected by a piezoelectric

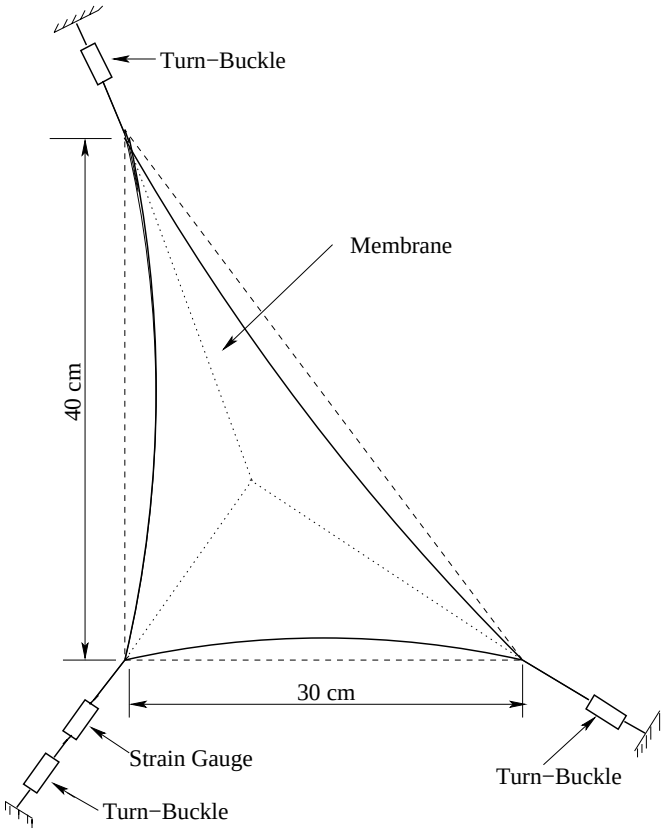

Figure 5.1: Membrane test model.

force transducer built into the hammer-tip and passed to the oscilloscope through an amplifier. The instantaneous velocity response of the membrane surface at the target point was measured by a Polytec OFV 3000 vibrometer controller. The output signals were also monitored on the oscilloscope and then both signals were sent to a data-logging computer and analysed using a MATLAB program. A schematic diagram of the above set-up is shown in Figure 5.2 and a view of the experimental set-up is shown in Figure 5.3..

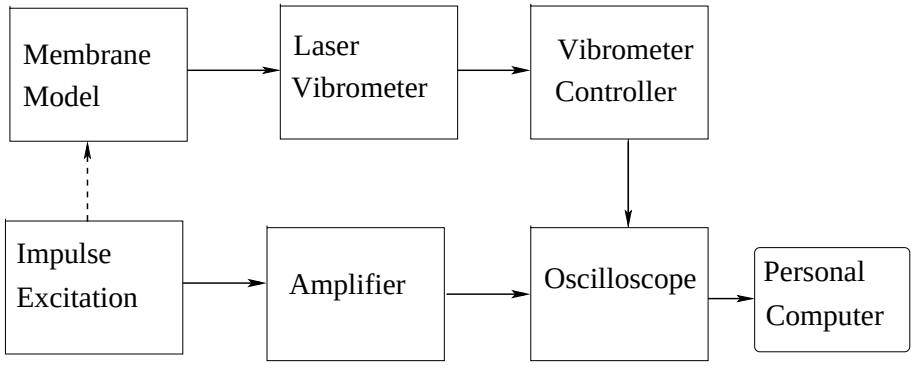

Figure 5.2: Schematic diagram of experimental set-up for impulse excitation.

The experimental procedure was as follows. Initially the laser vibrometer was focused on a target point on the membrane, which marked with Tipp-Ex to reflect laser signals. It was ensured that the laser vibrometer was receiving most of the reflected signal from the membrane by observing the indicator lights on the vibrometer. Then, an impulse was applied to the membrane while input and output signals were collected by the data-logging program. A set of fifty repeated measurements were made under similar conditions. Each set of readings was carefully monitored during data-logging to avoid poor measurements due to signal overload (saturation) and multiple impacts. Then, the Fast Fourier Transform (FFT) of the above signals was computed in order to obtain the FRF and the coherence functions of the input and output signals. The coherence function was helpful to ensure that the quality of the frequency response measurements was good enough. The natural frequencies were obtained from the FRF plot. The results of the above analysis are presented in section 5.3.

Figure 5.3: Experiment set-up for impulse excitation.

5.2.3 Mode Shapes

The membrane model was placed under a loudspeaker as shown in Figure 5.4. The loudspeaker was set to provide a sine wave input at a constant amplitude, and the frequency of which was varied slowly but continuously through the range from 10 Hz to 100 Hz. At the same time, lightweight powder (tea leaves) was spread uniformly on the surface of the membrane. The sine wave frequency was increased slowly from 10 Hz to a frequency where the membrane reaches a steady-state response condition. This frequency is the resonant frequency, close to the natural frequency of the membrane. At this frequency the powder moved away from these parts of the membrane that were experiencing the largest acceleration,

and tended to collect along the nodal lines, where the response was zero, of the particular mode shape that had been excited. After clearing the position of the nodal lines, the frequency was again increased gradually until the next resonant frequency was obtained. Further explanation to the slow sine sweep method can be obtained from Ewins [12]. A view of the experimental set-up is shown in Figure 5.4.

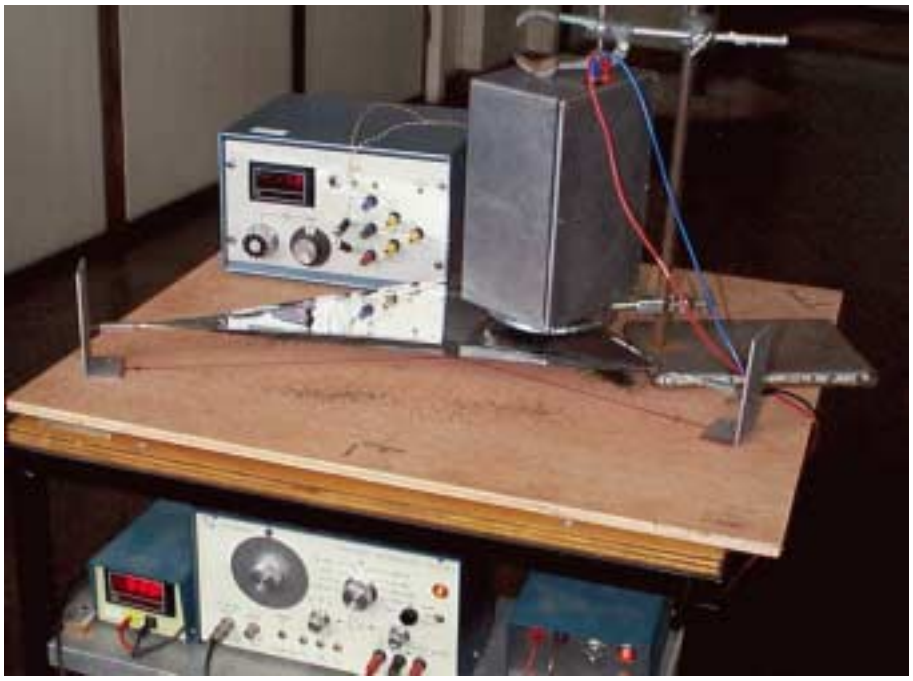

Figure 5.4: Experiment set-up for noise excitation.

5.3 Results and Discussion

5.3.1 Results

Figure 5.5 shows the Phase vs. Frequency, FRF and Coherence function plots for the experiment done using the laser vibrometer. The coherence function in Figure 5.5(c) shows the quality of the frequency response measurements. It is noted that the coherence function is approximately equal to 0.9, except in the vicinity of the anti-resonance frequencies and before the first natural frequency. The lower value of the coherence function in these regions is due to the low level of the response signal. This may well explain the reasons for noisy appearance in these regions. Therefore, the coherence function ensures the quality of the experimental frequency response is good enough.

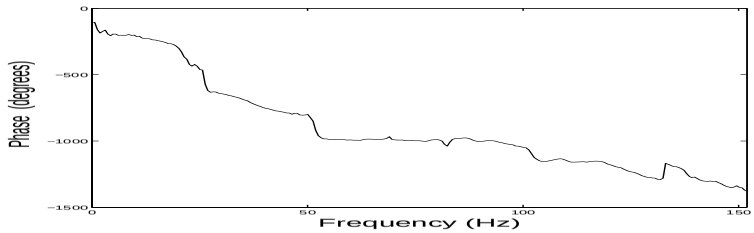

(a) Phase Diagram

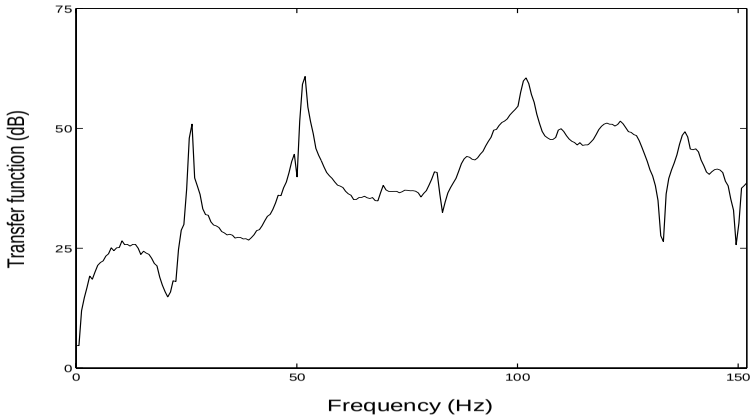

(b) Frequency Response Function

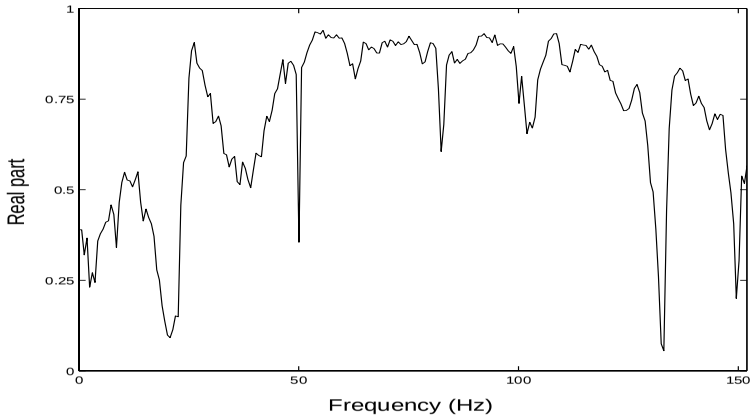

(c) Coherence Function

Figure 5.5: Phase, FRF and Coherence plots.

Figure 5.6 shows the plots of logarithmic, real and imaginary magnitude of the frequency response versus frequency. In the figure, the natural frequencies can be identified when the logarithmic magnitude plot and the real magnitude plot reach a peak and the imaginary magnitude plot passes through zero. The natural frequencies were obtained manually by looking for the above characteristics in

the frequency response function diagrams and have been tabulated in Table 5.2. The natural frequencies can also be found from the coherence and phase diagram in Figure 5.5.

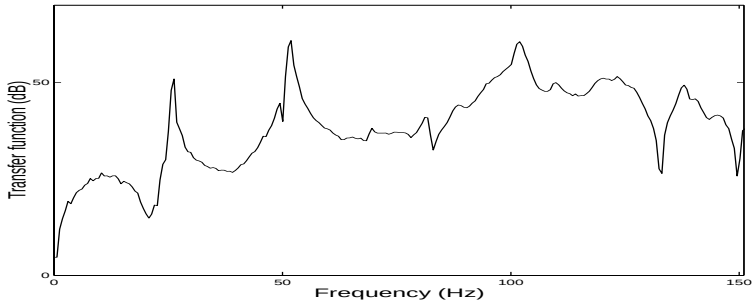

(a) Logarithmic FRF Diagram

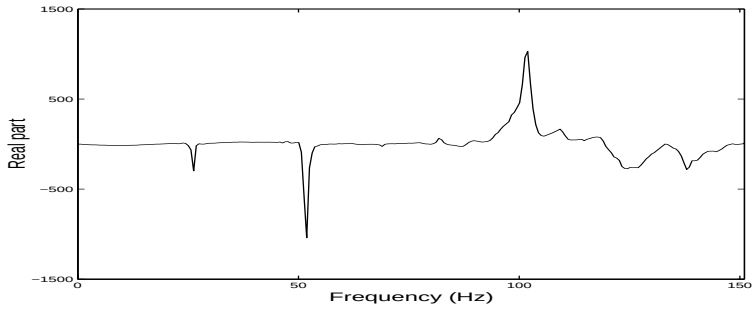

(b) Real parts of FRF Diagram

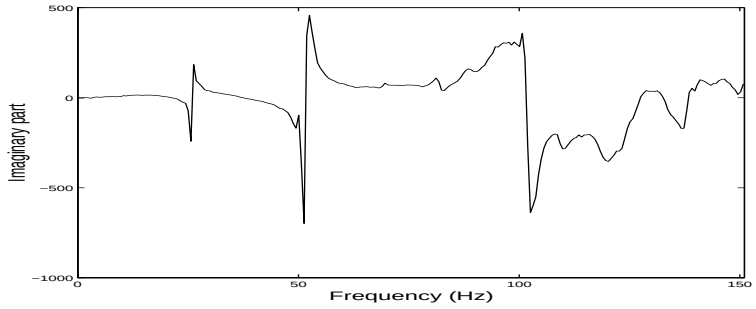

(c) Imaginary parts of FRF Diagram

Figure 5.6: Log, Real and Imaginary FRF plot of the model

It is noted in Figures 5.5 and 5.6 that only very few natural frequencies match all of the above criteria.

The natural frequencies of the experimental model were estimated using ABAQUS and have also been tabulated in Table 5.2, together with the natural frequencies observed in the loudspeaker test.

Table 5.2: Experimental and finite element results of the membrane.

Mode	Natural Frequency (Hz)		
	FE Method	Impulse Excitation	Slow Sine Sweep
1	36.3	25.6	26
2	58.6	48.8	49
3	63.8	51.3	51
4	67.7	65.3	62
5	82.4	69.6	69
6	88.3	80.6	80
7	90.8	84.2	84
8	94.9	87.9	87
9	99.2	91.6	92
10	105.8	94.6	94
11	109.8	100.7	100
12	114.5	—	105
13	117.9	108.6	109
14	120.1	113.5	113

The node lines of each mode shape have been plotted using a program written in MATLAB [27], and are plotted in Figure 5.7. The mode shape patterns observed in the loudspeaker test were compared with Figure 5.7.

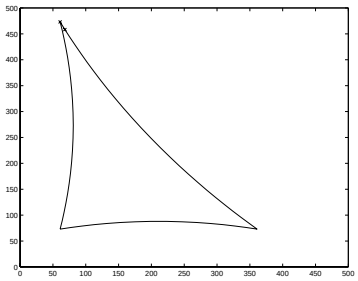

(a) Mode 1 (36.303 Hz)

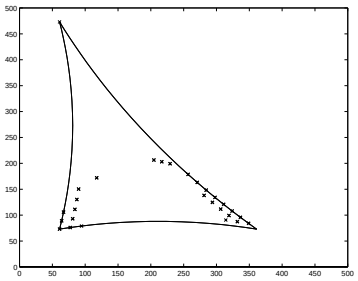

(b) Mode 2 (58.595 Hz)

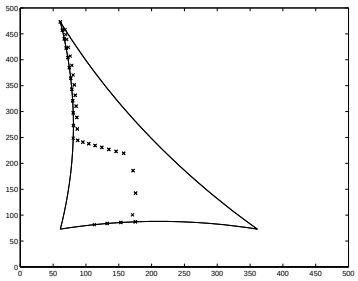

(c) Mode 3 (63.759 Hz)

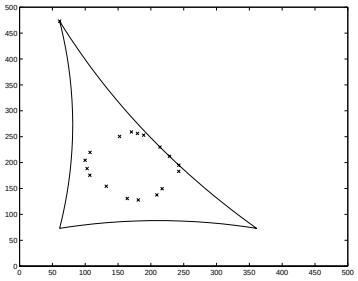

(d) Mode 4 (67.679 Hz)

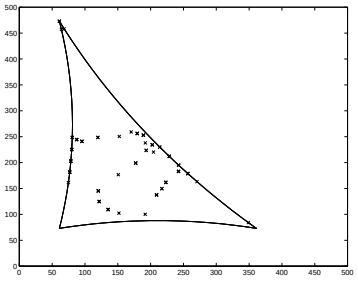

(e) Mode 5 (82.363 Hz)

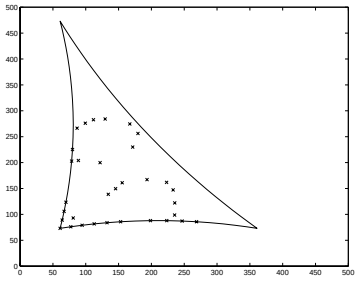

(f) Mode 6 (88.255 Hz)

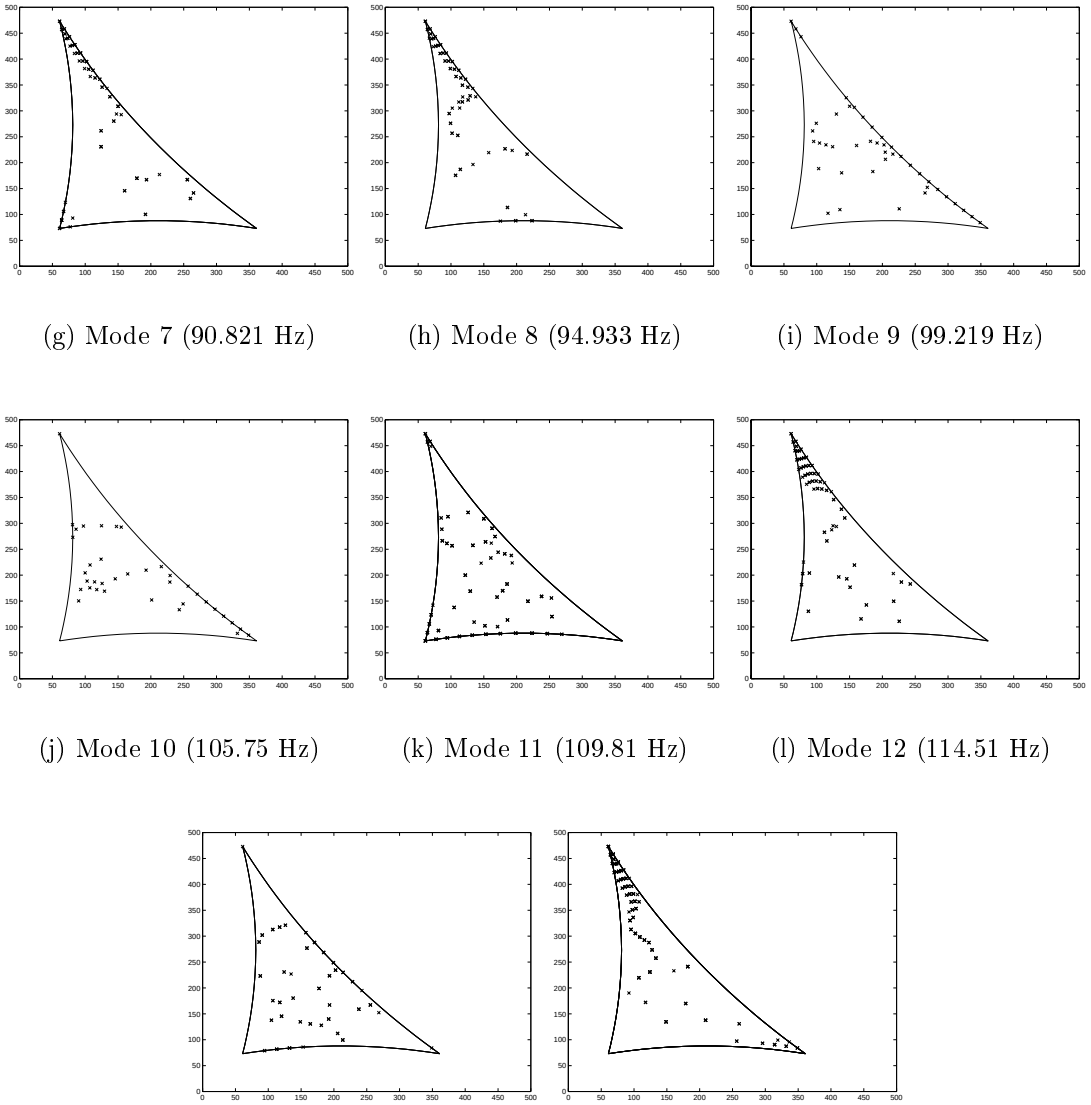

(g) Mode 7 (90.821 Hz) (h) Mode 8 (94.933 Hz) (i) Mode 9 (99.219 Hz)

(j) Mode 10 (105.75 Hz) (k) Mode 11 (109.81 Hz) (l) Mode 12 (114.51 Hz)

(m) Mode 13 (117.94 Hz) (n) Mode 14 (120.06 Hz)

Figure 5.7: Nodal lines of mode shapes of model at 20 N/m tension in vacuum.

5.3.2 Discussion

Table 5.2 presents a comparison between the natural frequencies of the model from the above three methods. It is observed that both impulse excitation (hammer) and slow sine sweep (loudspeaker) methods give similar values for the natural frequencies although there are a few discrepancies between them. However both of these results differ significantly from the numerical results obtained from ABAQUS. Because, the ABAQUS analysis ignores air effects, it should be compared with experiments done in vacuum conditions, but our experiments were done in atmospheric pressure. This suggests that atmospheric pressure plays a

vital role in the vibration of the membrane model; a considerable decrease of the lower natural frequencies is observed in the experiment results. At the higher frequencies the reduction is less, which indicates that air effects depend on the structural wave length. This effect is studied more clearly in the next chapter.

The loudspeaker model test was not successful because the experimental model is too small to observe clearly, the node lines corresponding to the mode shapes in the test. Anyhow, the loudspeaker experiment was helpful to compare the natural frequencies obtained in the laser vibrometer experiment.

Chapter 6

Air-Structure Interaction

This chapter investigates the effects of air-structure interaction on the vibration of a structure. Air-structure interaction is studied for an infinite flat membrane lying on an infinite baffle, using the solution available in Junger and Feit [20]. An experimental study of Sewall et al. [35] for a flat membrane in vacuum and various atmospheric pressures, in a vacuum chamber is considered. The above analytical solutions are applied to predict the natural frequencies of the model analysed by Sewall et al. Section 6.1 gives a brief introduction to air-structure interaction. The analytical study of an infinite flat membrane is explained in section 6.2. Section 6.3 presents a comparison between the results in Sewall et al. and various simple prediction schemes; the comparison is extended to the experimental model presented in Chapter 5.

6.1 Introduction

The experimental results in Chapter 5 show the importance of the surrounding medium on the vibration analysis. A similar study [35] done in a vacuum chamber at various air pressures had already indicated the effects of air mass on membrane vibration.

During vibration a membrane causes the surrounding medium to vibrate. This results in additional inertia forces or radiation according to a criterion specified in the following section. Hence the problem is of coupling between the fluid and the structure. This is a complex analytical approach and as indicated in section 2.4.3, many researchers have contributed to an understanding of this problem. However, there is yet no direct solution method available. An approximate solution will be obtained, from the references indicated in Chapter 2, and applied to predict the natural frequencies at various air pressures.

6.2 Analytical Approach

An analytical approach to the membrane-air interaction problem are discussed for an infinite plane membrane. The air effect on the membrane depends on the membrane surface wavelength and the acoustic wavelength. If the acoustic wavelength λ is greater than the surface wavelength λ_s, the pressure decays exponentially with distance from the membrane and no energy is radiated. In this case the air effect can be expressed as an additional mass on the membrane. If the acoustic wavelength is less than the surface wavelength, the effect would be a pure radiation.

The following important parameters are defined as follows. The membrane wave number k_s, the membrane flexural wave velocity c_m and acoustic wave number k are defined as

$$k_s^2 = \frac{m\omega^2}{T} \tag{6.1}$$

$$c_m = \sqrt{\frac{T}{m}} \tag{6.2}$$

$$k = \frac{\omega}{c} \tag{6.3}$$

where T is the force in the membrane, c the sound velocity, and m the surface density of the membrane.

As explained in Chapter 2, the added mass derived in section 2.4.3 is valid only for an infinite flat membrane. It is impossible to find an simple analytical solutions to a finite membrane, therefore the added mass expression of infinite membrane will be used in this chapter for the finite flat membrane to find its natural frequencies and mode shapes. In the case of air on one side of the infinite membrane only, the added air mass would be

$$m_a \approx \frac{\rho}{k_s}, \quad \text{for} \quad k_s \gg k \tag{6.4}$$

In the case of air on both sides of the infinite membrane, this becomes, obviously

$$m_a \approx \frac{2\rho}{k_s} \tag{6.5}$$

Assuming that mode shapes of the membrane remain unchanged, a particular natural frequency of the membrane in air is calculated from the natural frequency in vacuum (e.g. from ABAQUS) as follows

$$f_a = f\sqrt{\frac{M_{MG}}{M_{MG} + M_{AG}}} \tag{6.6}$$

where M_{MG} is the generalised mass of the membrane and M_{AG} is the generalised mass of the air for the chosen model. f_a is the natural frequency of the membrane in air and f its natural frequency in vacuum.

For example, in the case of Sewall et al.'s model, the thin membrane vibrating in air at atmospheric pressure with in-plane tension of 33 N/m and surface density of 0.01758 kg/m^2, the membrane wave velocity c_m is calculated as 43.33 m/s and the velocity of sound c is 344 m/s. The fluid loading parameter ϵ is calculated for the fundamental natural frequency of 27 Hz as

$$\epsilon \approx 141 \tag{6.7}$$

Therefore, it indicates that the fluid loading is very important in estimation of the natural frequencies on this model.

And, k_s/k is calculated as

$$\frac{k_s}{k} = \frac{c}{c_m} \approx 8 \tag{6.8}$$

Therefore

$$k_s \gg k \tag{6.9}$$

Defining the structure wave length $\lambda_s = 1/k_s$ and the air (acoustic) wave length $\lambda = 1/k$

$$\lambda_s \ll \lambda \tag{6.10}$$

Hence the membrane vibrating in air at atmospheric pressure will have surface wavelength smaller than the acoustic wavelength. As explained earlier, in this case air will have the effect of adding mass to the membrane surface, but there will be no radiation.

Therefore, Sewall et al.'s model is analysed in section 6.3.1 for natural frequencies and mode shapes using the air mass expressions derived in this section. Section 6.2.1 gives the more practical way of using Equation (6.6).

6.2.1 Practical Implementation

To apply Equation (6.6) for a particular membrane structure we proceed as follows. First we estimate the natural frequencies using ABAQUS. For each mode the generalised mass M_{MG} is obtained from the ABAQUS result files. The added air mass m_a is then calculated from either Equation (6.4) or (6.5), and then the corresponding generalised air mass M_{AG} is calculated as

$$M_{AG} = \int\int m_a \psi^2_{(x,y)} \mathrm{d}x\mathrm{d}y \tag{6.11}$$

where ψ is the mode shape in vacuum, obtained from ABAQUS. In Equation (6.11), m_a is constant throughout the membrane surface. Therefore, by considering one integration point for each triangular element, Gauss Quadrature [3] of Equation (6.11) gives

$$M_{AG} = m_a \sum \psi_i^2 A_i \tag{6.12}$$

In Equation (6.12), ψ_i is the component of the eigenvector at the integration point of element i. Because only the values of the eigenvectors of the nodes of the model can be directly obtained from the ABAQUS result files, Equation (6.12), is modified to

$$M_{AG} = m_a \boldsymbol{\psi}^T \mathbf{A} \boldsymbol{\psi} \tag{6.13}$$

where $\mathbf{A}$ is the *lumped area matrix* of the nodal points and $\boldsymbol{\psi}$ is the eigenvector of the nodal points.

The generalised masses of the air mass are calculated using a simple program written in MATLAB from the Equation (6.13).

6.3 Comparison of Analytical and Experimental Results

Results from both the experiment in Chapter 5 and Sewall et al. are compared with the analytical results obtained from the method described in the previous section.

6.3.1 Sewall et al.'s Model

(a) Membrane in Vacuum with Apex Tension of 142 N

Sewall et al.'s experimental model has been analysed in ABAQUS; the node lines for the first nine modes are plotted in Figure 6.1.

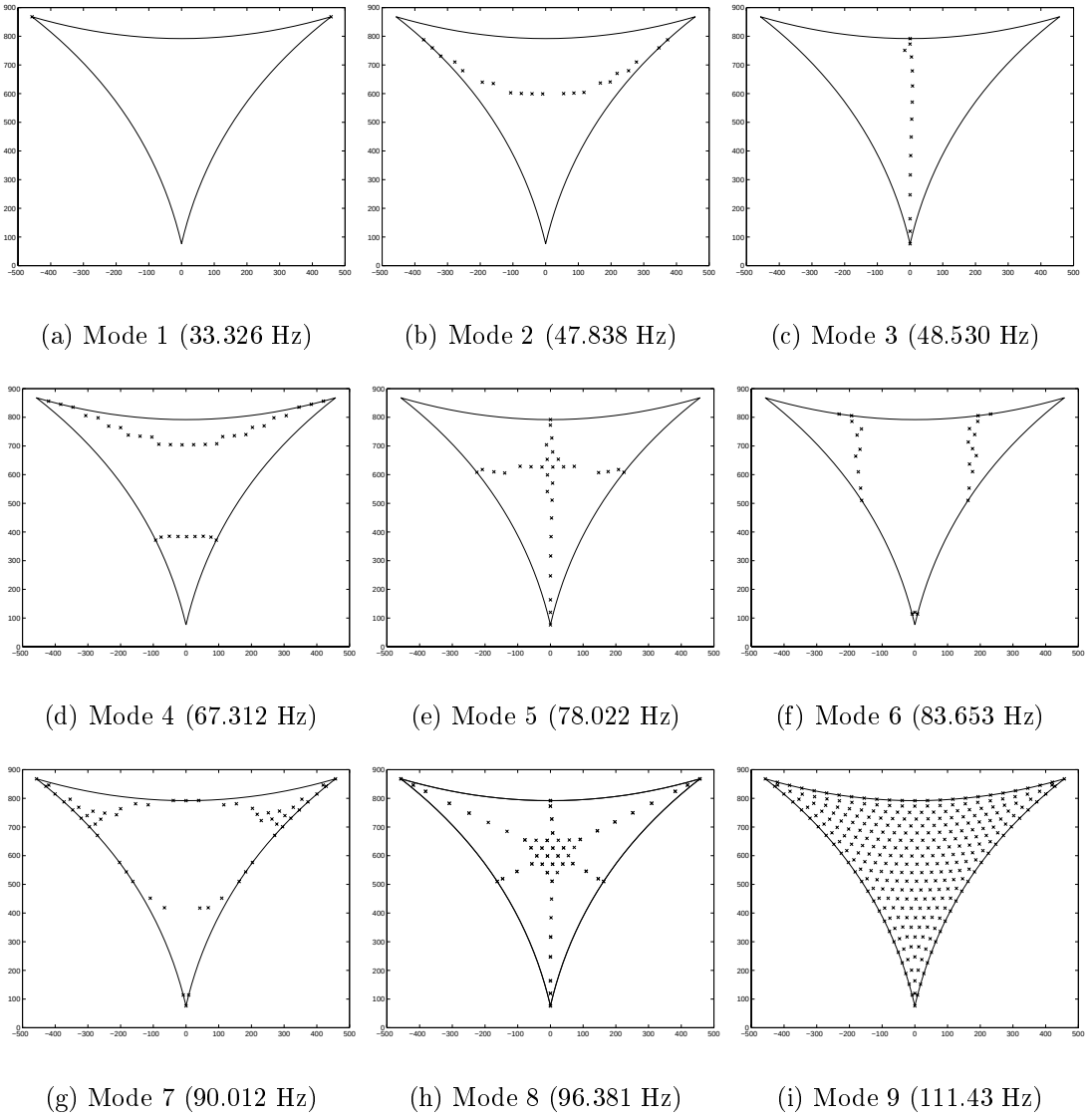

(a) Mode 1 (33.326 Hz) (b) Mode 2 (47.838 Hz) (c) Mode 3 (48.530 Hz)

(d) Mode 4 (67.312 Hz) (e) Mode 5 (78.022 Hz) (f) Mode 6 (83.653 Hz)

(g) Mode 7 (90.012 Hz) (h) Mode 8 (96.381 Hz) (i) Mode 9 (111.43 Hz)

Figure 6.1: ABAQUS mode shapes (in vacuum) for Sewall at al.'s model; 142 N apex tension.

Figure 6.1 can be compared with the the corresponding mode shapes experimentally obtained by Sewall et al. in vacuum (Figure 6.2).

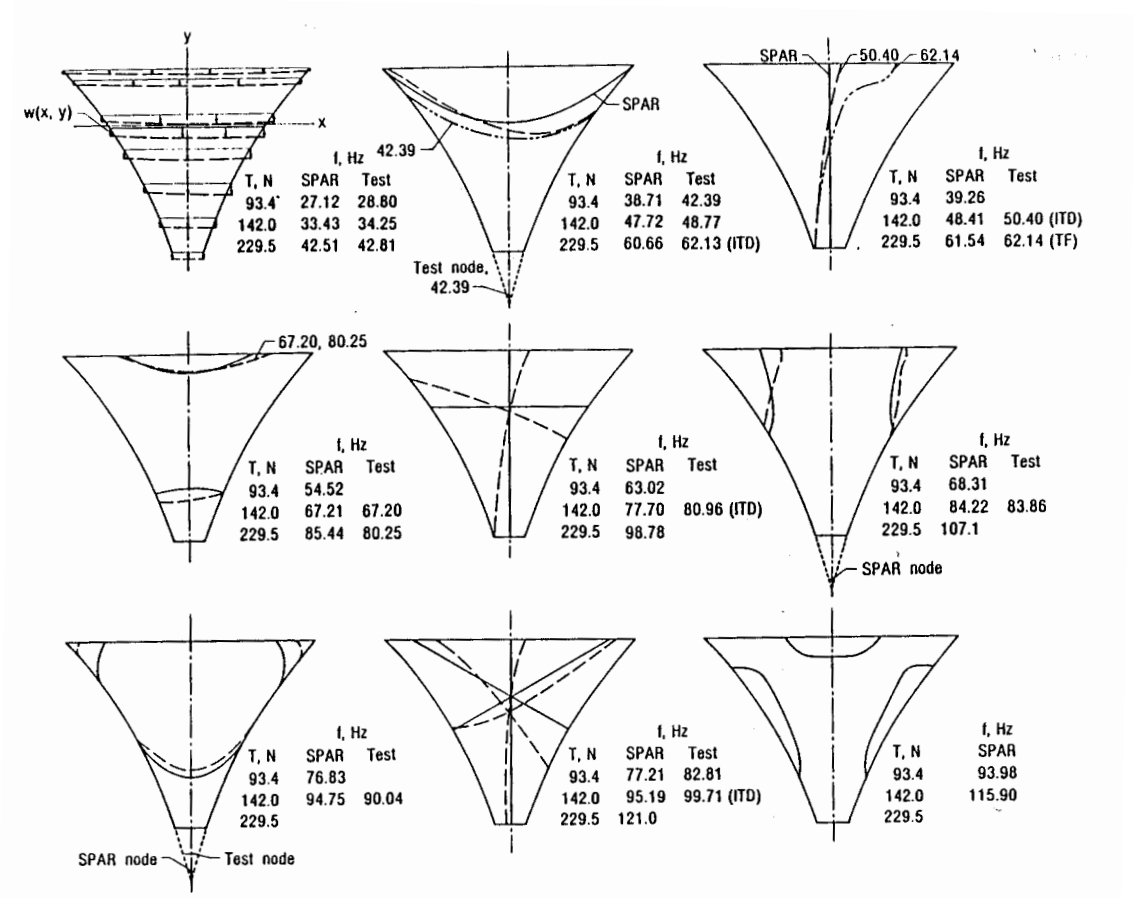

Figure 6.2: Experimental mode shapes in vacuum; apex tension 142 N (from Sewall et al. [35]).

Figures 6.1 and 6.2 are in good agreement for the first eight mode shapes. Note that Figure 6.2 shows both the numerical (SPAR FE Package) and experimental results in Sewall et al. [35]. The ABAQUS mode shapes in Figure 6.1 and the SPAR mode shapes (solid line) in Figure 6.2 have identical patterns; corresponding modes have very close natural frequencies. But, the experimental nodal line patterns in Figure 6.2 show a slight difference from the numerical nodal line patterns; the numerical nodal lines have clear symmetric patterns, but the experimental nodal lines are slightly asymmetric. Also, the experimental natural frequencies differ slightly from the numerical frequencies. These results show that Sewall et al.'s model has small imperfection because of either manufacturing or material tolerances. The figures suggest that the experimental results at any pressures should also be reliable for further comparison purposes.

(b) Air at 0.61 atm on One Side of Membrane with 93.4 N Apex Tension.

Table 6.1 shows the natural frequency calculation steps for the test at 0.61 atm pressure and 93.4 N equal apex tension load. In this case, air mass is calculated by assuming that air is present only on one side of the membrane surface.

Table 6.1: Vibration at 0.61 atm with 93.4 N equal apex load with air on one side.

Mode	$1/k_s$	m_a	Generalised Mass (kg)			Natural Frequency (Hz)		
	(m)	(kg/m^2)	M_{MG}	M_{AG}	M_{MG+AG}	FE dry	FE wet	Exp.
1	0.255	0.191	0.01571	0.02805	0.04376	27.029	16.195	16.31
2	0.178	0.133	0.01009	0.00655	0.01664	38.801	30.214	30.95
3	0.175	0.131	0.01244	0.00840	0.02084	39.363	30.412	32.50
4	0.126	0.094	0.03198	0.00630	0.03828	54.595	49.901	37.05
5	0.109	0.082	0.01135	0.00370	0.01505	63.279	54.953	47.84
6	0.102	0.076	0.00399	0.00400	0.00799	67.852	47.949	52.77
7	0.094	0.071	0.00101	0.00260	0.00361	73.025	38.626	80.51
8	0.088	0.066	0.01661	0.00255	0.01916	78.167	72.875	84.08
9	0.071	0.053	0.01811	0.00000	0.01811	91.689	91.689	
10	0.074	0.055	0.00213	0.00150	0.00363	93.410	71.553	
11	0.072	0.054	0.00136	0.00225	0.00361	96.537	59.253	
12	0.070	0.052	0.00122	0.00195	0.00317	98.854	61.326	
13	0.062	0.047	0.00124	0.00135	0.00259	110.59	76.520	
14	0.062	0.046	0.00127	0.00115	0.00242	111.08	80.469	
15	0.057	0.043	0.00192	0.00175	0.00367	120.65	87.269	

Column 8 of the table gives the analytical predictions for the natural frequencies ("wet") at 0.61 atm, whereas natural frequencies in vacuum ("dry") are in column 7. The natural frequencies in column 8 have been calculated from Equation 6.6. Column 8 shows that the order of the modes has changed.

Table 6.2 tabulates the experimental and analytical natural frequencies after re-arranging the modes. Column 2 of Table 6.2 lists, in ascending order, the same values of column 8 of Table 6.1, and it indicates, in bracket, the mode order in vacuum.

Table 6.2 shows almost identical values for the first six modes. In fact, the last two experimental natural frequencies in Table 6.2 are arranged according to the nodal line patterns of the corresponding mode shapes, Figures 6.3 and 6.4, because the experimental data does not include all natural frequencies of the model.

The nodal lines in the changed mode order give the mode shapes in air. Figure 6.3 plots them in the correct order at 0.61 atm. Figure 6.3 can be compared with the experimental nodal lines given in Sewall et al. [35], Figure 6.4.

Table 6.2: Vibration at 0.61 atm with 93.4 N equal apex load with air on one side only.

Mode	Natural Frequency (Hz)	
	Experimental	Analytical
1	16.31	16.20(1)
2	30.95	30.21(2)
3	32.50	30.41(3)
4	37.05	38.63(7)
5	47.84	47.95(6)
6	52.77	49.90(4)
7	—	54.95(5)
8	—	59.25(11)
9	—	61.33(12)
10	80.51	71.55(10)
11	—	72.88(8)
12	—	76.52(13)
13	84.08	80.47(14)
14	—	87.27(15)
15	—	91.69(9)

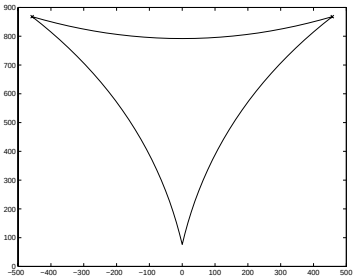

(a) Mode 1 (16.213 Hz)

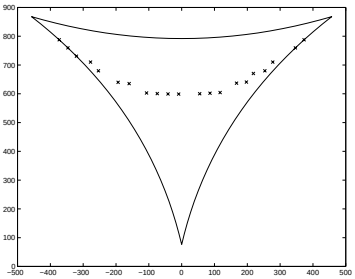

(b) Mode 2 (30.169 Hz)

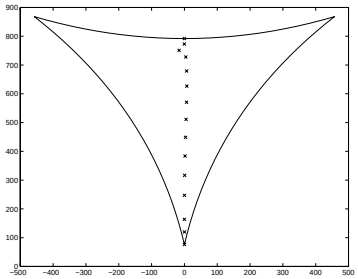

(c) Mode 3 (30.522 Hz)

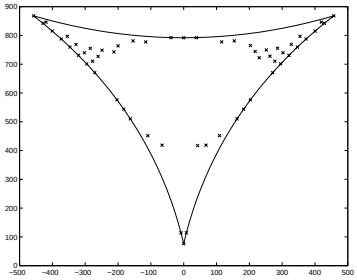

(d) Mode 7 (38.626 Hz)

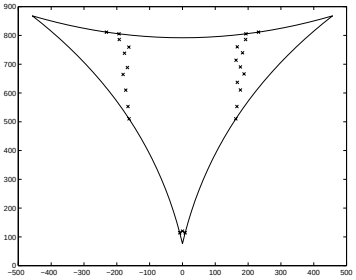

(e) Mode 6 (48.100 Hz)

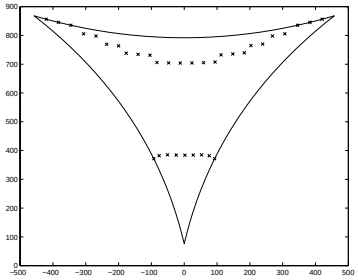

(f) Mode 4 (49.578 Hz)

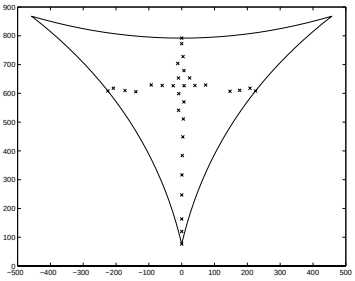

(g) Mode 5 (55.415 Hz)

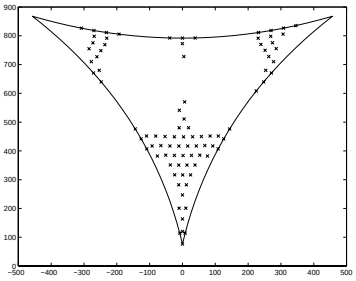

(h) Mode 11 (59.668 Hz)

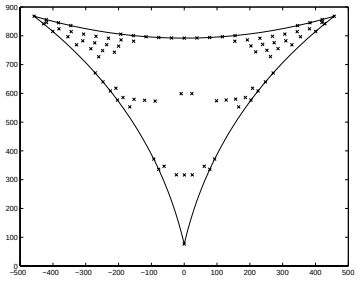

(i) Mode 12 (61.326 Hz)

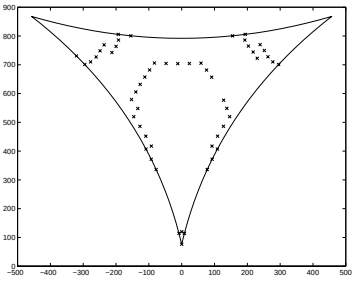

(j) Mode 10 (72.051 Hz)

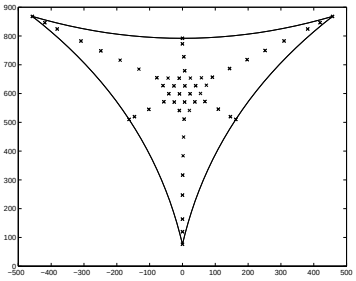

(k) Mode 8 (72.875 Hz)

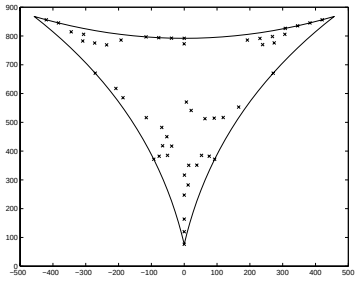

(l) Mode 13 (76.520 Hz)

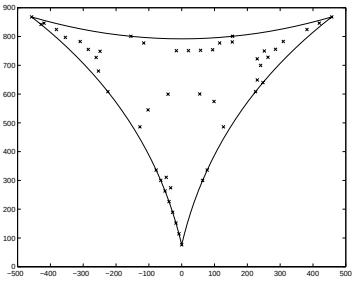

(m) Mode 14 (80.469 Hz)

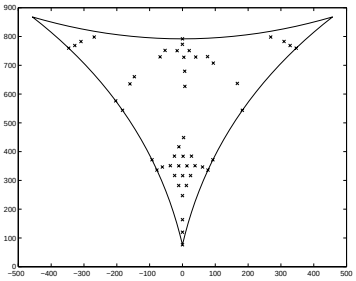

(n) Mode 15 (72.481 Hz)

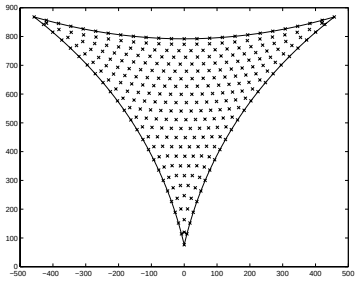

(o) Mode 9 (91.689 Hz)

Figure 6.3: Mode shapes at 93.4 N apex tension at 0.61 atm.

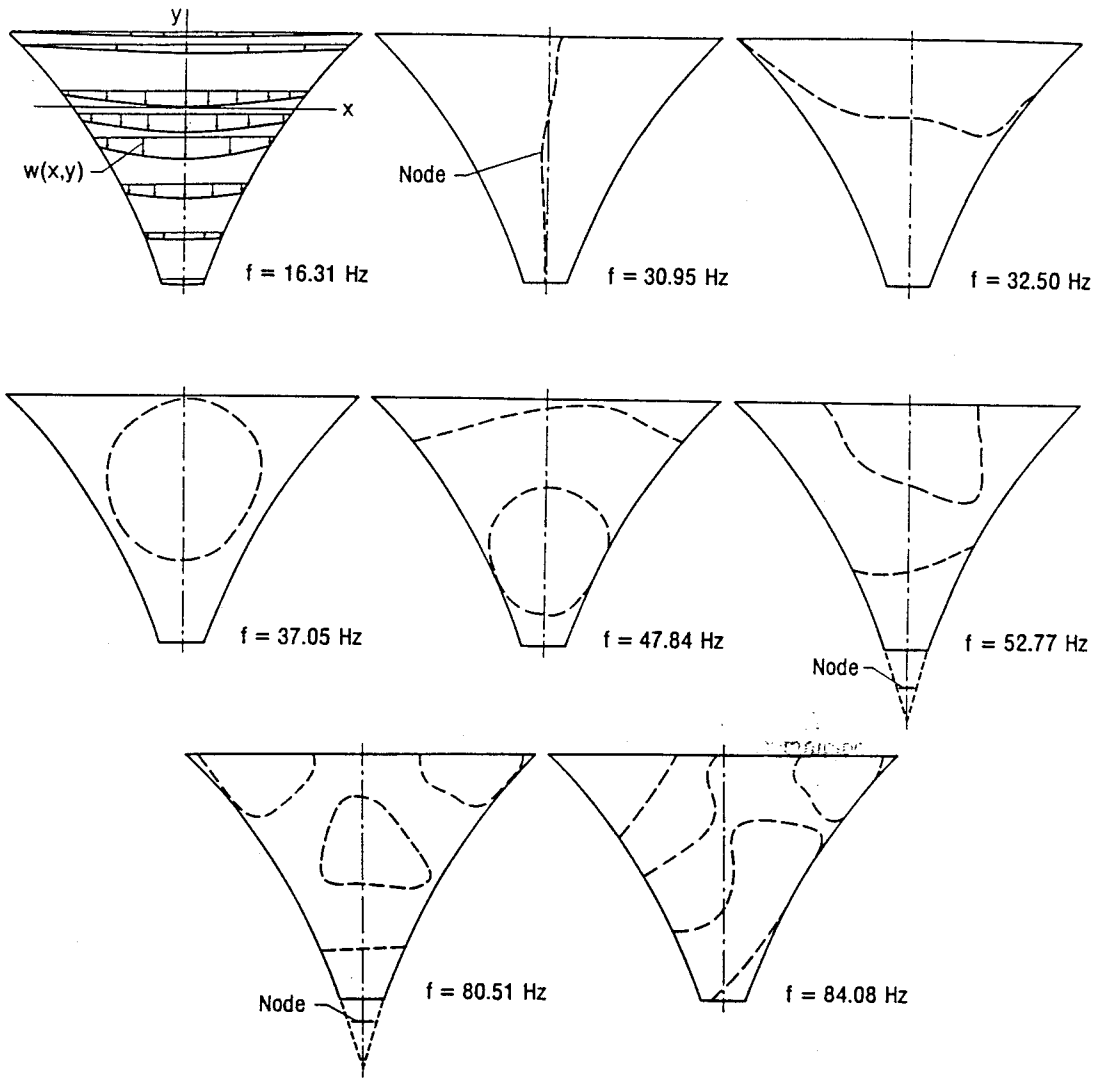

Figure 6.4: Experimental mode shapes at 93.4 N apex tension in 0.61 atm (from Sewall et al. [35]).

Figures 6.3 and 6.4 are in fairly good agreement in most cases. Mode 5 shows a poor correlation. Modes 2 and 3 have to be interchanged with one another. The natural frequencies of modes 10 and 12 are placed according to the nodal line patterns although there are disagreements in the natural frequency values. The numerical nodal lines have a symmetric patterns, but the experimental nodal lines have a slight asymmetric nature.

(c) Air at 0.61 atm on Two Sides of Membrane, 93.4 N Apex Tension

Table 6.3 shows the natural frequency calculation steps for the test with 0.61 atm pressure and 93.4 N tensions at the apex. In this case, the air mass is calculated by assuming that air is on both sides of the membrane surface.

Table 6.3: Vibration at 0.61 atm with 93.4 N equal apex load with air on two sides.

Mode	$1/k_s$ (m)	m_a (kg/m^2)	Generalised Mass (kg)			Natural Frequency (Hz)		
			M_{MG}	M_{AG}	M_{MG+AG}	FE dry	FE wet	Exp.
1	0.255	0.381	0.01571	0.0561	0.07181	27.029	12.642	16.31
2	0.178	0.266	0.01009	0.0131	0.02319	38.801	25.594	30.95
3	0.175	0.262	0.01244	0.0168	0.02924	39.363	25.675	32.50
4	0.126	0.189	0.03198	0.0126	0.04458	54.595	46.240	37.05
5	0.109	0.163	0.01135	0.0074	0.01875	63.279	49.233	47.84
6	0.102	0.152	0.00399	0.0080	0.01199	67.852	39.142	52.77
7	0.094	0.141	0.00101	0.0052	0.00621	73.025	29.450	80.51
8	0.088	0.132	0.01661	0.0051	0.02171	78.167	68.372	84.08
9	0.071	0.106	0.01811	0.0000	0.01811	91.689	91.689	
10	0.074	0.110	0.00213	0.0030	0.00513	93.410	60.190	
11	0.072	0.107	0.00136	0.0045	0.00586	96.537	46.507	
12	0.070	0.104	0.00122	0.0039	0.00512	98.854	48.255	
13	0.062	0.093	0.00124	0.0027	0.00394	110.59	62.041	
14	0.062	0.092	0.00127	0.0023	0.00357	111.08	66.253	
15	0.057	0.085	0.00192	0.0035	0.00542	120.65	71.809	

Column 8 of the table gives the analytical predictions for the natural frequency at 0.61 atm from the vacuum natural frequencies, in column 7 of the table. The natural frequencies in column 8 are calculated from Equation 6.6. Note that the order of the "wet" modes differ from those of the "dry" modes.

The wet modes have been rearranged in Table 6.4. Column 2 of the table indicates, in bracket, the mode orders in vacuum.

Table 6.4: Vibration at 0.61 atm with 93.4 N equal apex load with air on two sides.

Mode	Natural Frequency (Hz)	
	Experimental	Analytical
1	16.31	12.64(1)
2	30.95	25.59(2)
3	32.50	25.68(3)
4	37.05	29.45(7)
5	47.84	39.14(6)
6	52.77	46.24(4)
7	—	46.51(11)
8	—	48.26(12)
9	—	49.23(5)
10	80.51	60.19(10)
11	—	62.04(13)
12	84.08	66.25(14)
13	—	68.37(8)
14	—	71.81(15)
15	—	91.69(9)

Table 6.4 shows smaller values of the analytical natural frequencies for all modes. This shows that the air mass that has been used in the analysis is too large. The last two experimental natural frequencies in Table 6.4 are arranged according to the nodal line patterns of the corresponding mode shapes plotted in figures 6.3 and 6.4, because the experimental data does not include all the natural frequencies of the model.

(d) Air at 1 atm on One Side of Membrane, 93.4 N Apex Tension

Table 6.5 shows the natural frequency calculation steps for the test with air at pressure of 1 atm and 93.4 N tension load at the apexes. In this case, air mass is calculated by assuming that air is only on one side of the membrane surface.

Table 6.5: Vibration with air on one side at 1 atm, 93.4 N equal apex load.

Mode	$1/k_s$ (m)	m_a (kg/m^2)	Generalised Mass (kg)			Natural Frequency (Hz)		
			M_{MG}	M_{AG}	M_{MG+AG}	FE dry	FE wet	Exp.
1	0.255	0.625	0.01571	0.04600	0.06171	27.029	13.638	13.94
2	0.178	0.436	0.01009	0.01075	0.02084	38.801	27.000	26.34
3	0.175	0.429	0.01244	0.01375	0.02619	39.363	27.129	28.90
4	0.126	0.310	0.03198	0.01030	0.04228	54.595	47.482	34.77
5	0.109	0.267	0.01135	0.00605	0.01740	63.279	51.107	43.14
6	0.102	0.249	0.00399	0.00655	0.01054	67.852	41.747	43.85
7	0.094	0.231	0.00101	0.00425	0.00526	73.025	32.000	45.84
8	0.088	0.216	0.01661	0.00415	0.02076	78.167	69.919	47.42
9	0.071	0.173	0.01811	0.0000	0.01811	91.689	91.689	52.12
10	0.074	0.181	0.00213	0.00245	0.00448	93.410	64.409	67.59
11	0.072	0.176	0.00136	0.00365	0.00501	96.537	50.297	71.78
12	0.070	0.171	0.00122	0.00315	0.00437	98.854	52.232	89.23
13	0.062	0.153	0.00124	0.00220	0.00344	110.59	66.397	
14	0.062	0.152	0.00127	0.00190	0.00317	111.08	70.309	
15	0.057	0.140	0.00192	0.00285	0.00477	120.65	76.545	

The natural frequencies in column 8 of Table 6.5 are calculated from Equation (6.6). Again, the mode order changes from vacuum and Table 6.6 gives the experimental and analytical natural frequencies in the changed mode orders.

Table 6.6: Vibration with air on one side at 1 atm, 93.4 N equal apex load.

Mode	Natural Frequency (Hz)	
	Experimental	Analytical
1	13.94	13.64(1)
2	26.34	27.00(2)
3	28.90	27.13(3)
4	34.77	32.00(7)
5	—	41.75(6)
6	43.14,43.85,45.84,47.42	47.48(4)
7	52.12	50.30(11)
8	—	51.11(5)
9	—	52.23(12)
10	—	64.41(10)
11	67.59	66.40(13)
12	—	69.92(8)
13	71.78	70.31(14)
14	—	76.55(15)
15	—	91.689(9)

Table 6.6 shows similar values for the natural frequencies at lower modes. The experimental natural frequencies in the table are arranged according to the nodal

line patterns of corresponding mode shapes plotted in Figures 6.5 and 6.6; again the experimental data does not have all natural frequencies of the model.

Figure 6.5 plots the nodal lines of the mode shapes at 1 atm, and is compared with the experimental nodal lines of corresponding mode shapes in Figure 6.6.

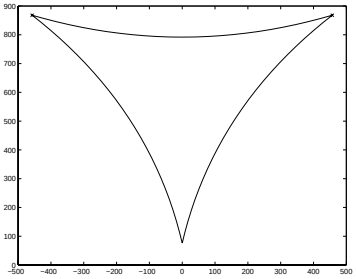

(a) Mode 1 (13.660 Hz)

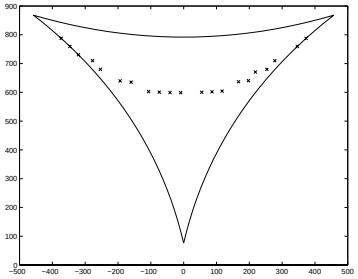

(b) Mode 2 (26.966 Hz)

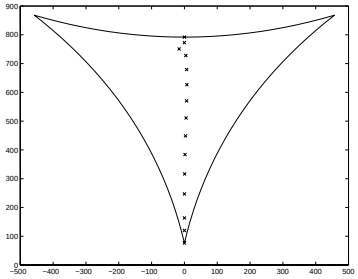

(c) Mode 3 (27.259 Hz)

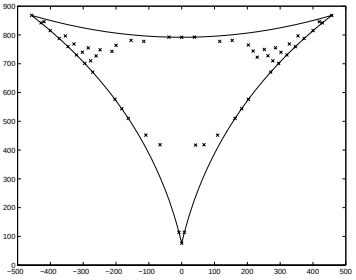

(d) Mode 7 (32.000 Hz)

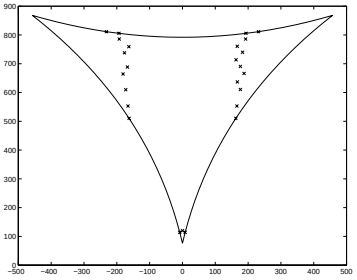

(e) Mode 6 (41.947 Hz)

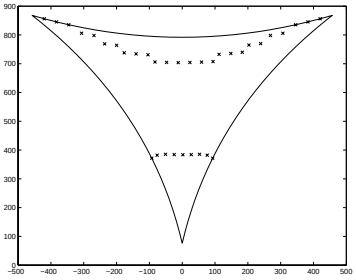

(f) Mode 4 (47.039 Hz)

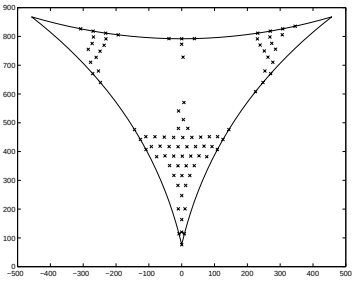

(g) Mode 11 (50.297 Hz)

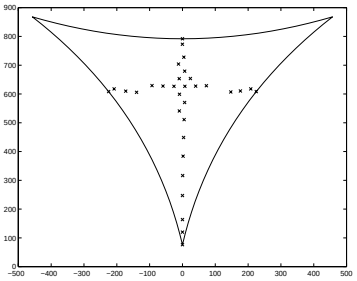

(h) Mode 5 (51.705 Hz)

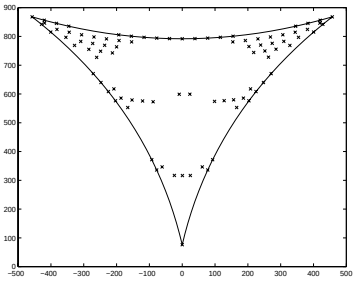

(i) Mode 12 (52.232 Hz)

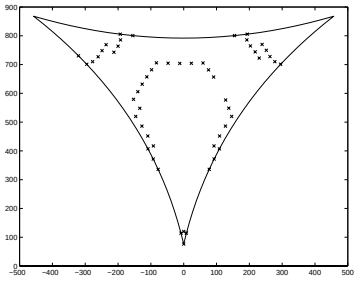

(j) Mode 10 (64.409 Hz)

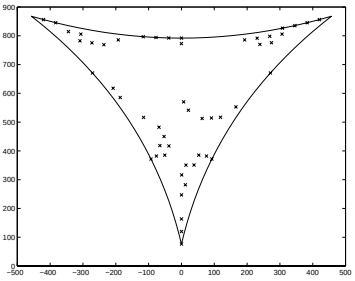

(k) Mode 13 (66.397 Hz)

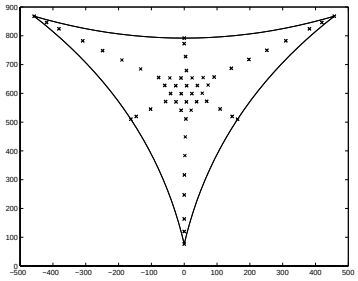

(l) Mode 8 (69.919)

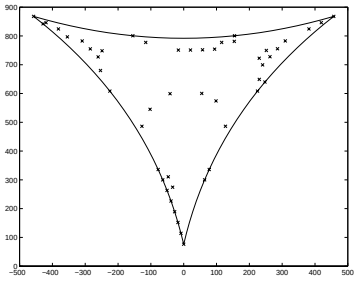

(m) Mode 14 (70.309 Hz)

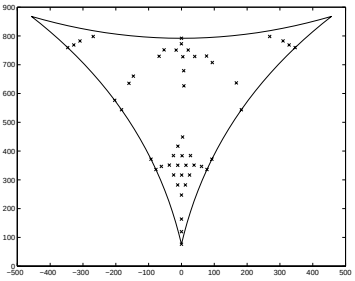

(n) Mode 15 (77.361 Hz)

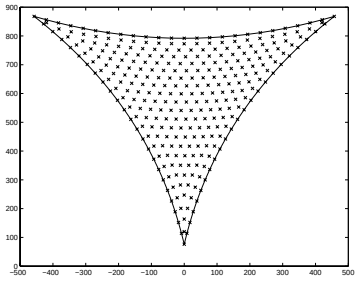

(o) Mode 9 (91.689 Hz)

Figure 6.5: Mode shapes at 1 atm with 93.4 N apex tension.

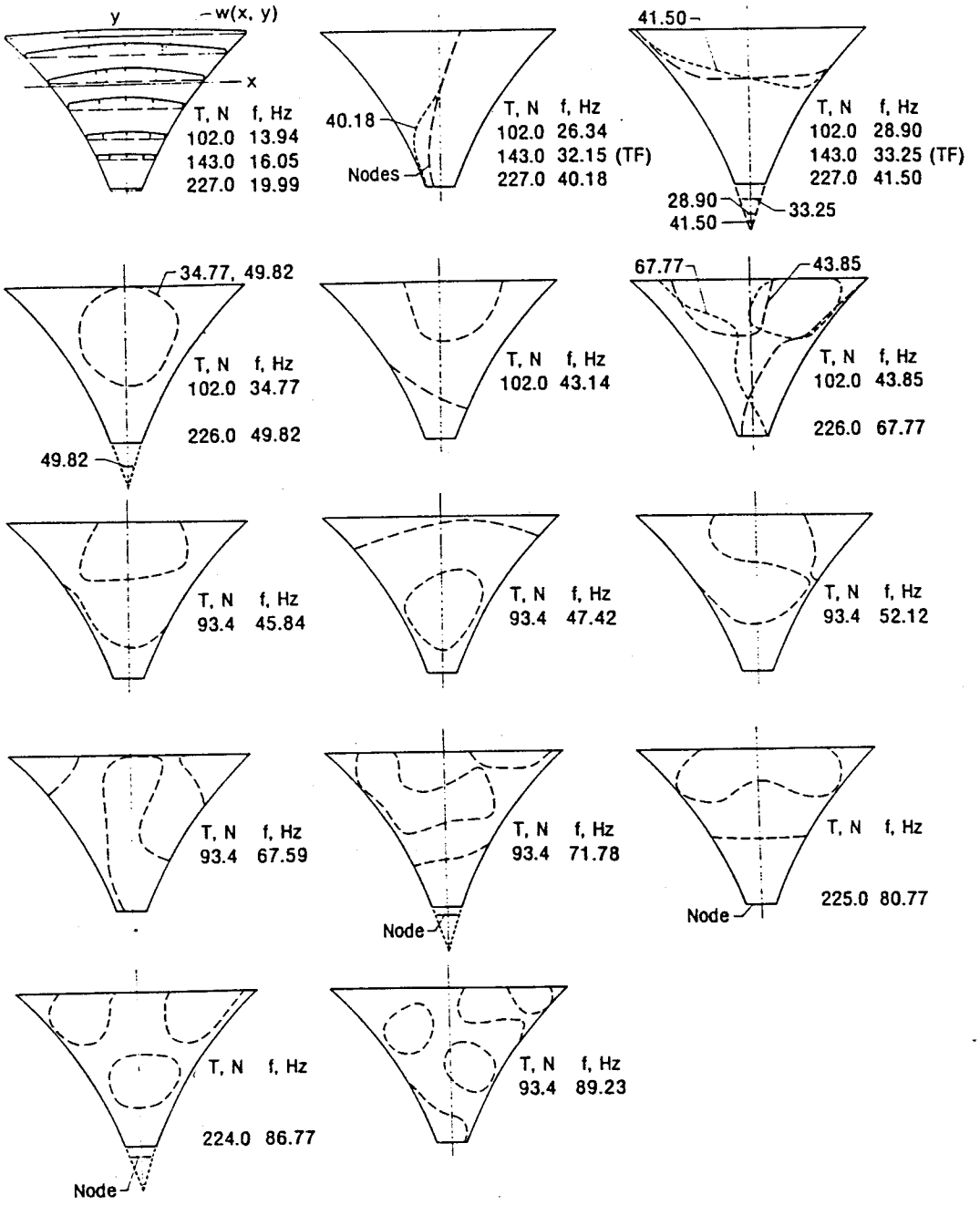

Figure 6.6: Experimental Mode shapes at 1 atm, 93.4 N apex tension (From Sewall et al. [35]).

Figures 6.5 and 6.6 can be compared as follows. For the lower modes the two figures show better agreement than for the higher modes. The numerical nodal lines have a symmetric pattern, but the experimental nodal lines have a slight asymmetric nature.

(e) Air at 1 atm on Two Sides of Membrane; 93.4 N Apex Tension.

Table 6.7 shows the natural frequency calculation steps for the model with 1 atm pressure and 93.4 N apex tension. In this case, air mass has been calculated by assuming that air is present on both sides of the membrane surface. The rearranged mode shapes is given in Table 6.8.

Table 6.7: Vibration at 1 atm with 93.4 N equal apex load with air on both sides of membrane.

Mode	$1/k_s$ (m)	m_a (kg/m^2)	Generalised Mass (kg)			Natural Frequency (Hz)		
			M_{MG}	M_{AG}	M_{MG+AG}	FE dry	FE wet	Exp.
1	0.255	0.625	0.01571	0.0920	0.10771	27.029	10.323	13.94
2	0.178	0.436	0.01009	0.0215	0.03159	38.801	21.929	26.34
3	0.175	0.429	0.01244	0.0275	0.03994	39.363	21.968	28.90
4	0.126	0.310	0.03198	0.0206	0.05258	54.595	42.578	34.77
5	0.109	0.267	0.01135	0.0121	0.02345	63.279	44.024	43.14
6	0.102	0.249	0.00399	0.0131	0.01709	67.852	32.785	43.85
7	0.094	0.231	0.00101	0.0085	0.00951	73.025	23.798	45.84
8	0.088	0.216	0.01661	0.0083	0.02491	78.167	63.829	47.42
9	0.071	0.173	0.01811	0.0000	0.01811	91.689	91.689	52.12
10	0.074	0.181	0.00213	0.0049	0.00703	93.410	51.417	67.59
11	0.072	0.176	0.00136	0.0073	0.00866	96.537	38.256	71.78
12	0.070	0.171	0.00122	0.0063	0.00752	98.854	39.817	89.23
13	0.062	0.153	0.00124	0.0044	0.00564	110.59	54.855	
14	0.062	0.152	0.00127	0.0038	0.00507	111.08	55.595	
15	0.057	0.140	0.00192	0.0057	0.00762	120.65	60.562	

Table 6.8: Vibration at 1 atm with 93.4 N equal apex load with air on two sides of membrane.

Mode	Natural Frequency (Hz)	
	Experimental	Analytical
1	13.94	10.32(1)
2	26.34	21.93(2)
3	28.90	21.97(3)
4	34.77	23.80(7)
5	—	32.79(6)
6	43.14, 43.85, 45.84, 47.42	38.26(11)
7	52.12	39.82(12)
8	—	42.58(4)
9	—	44.02(5)
10	—	51.42(10)
11	67.59	54.86(13)
12	—	55.60(14)
13	71.78	60.56(15)
14	—	63.83(8)
15	—	91.69(9)

As in section 6.3.1 (c) above, the Table shows that the analytical natural frequencies have been under-predicted for all modes. This shows that too large a value for the air mass has been used in the analysis.

6.3.2 Experimental Model

This section tabulates the analytical natural frequency calculation steps for the experimental model in Chapter 5. Similar calculation steps are followed as explained in section 6.3.1. In the model used by Sewall et al., it was observed that some of the intermediate modes were not tabulated from their experiment. But in the experiment described in Chapter 5, every mode up to 14 was taken without missing any intermediate modes. This is the reason why the following analysis is carried out.

(a) Air at 1 atm on One Side of Membrane

Table 6.9 shows the calculation steps for the model with 1 atm pressure and 20 N/m surface tension.

Table 6.9: Vibration at 1 atm with 20 N/m surface tension with air on one side.

Mode	$1/k_s$	m_a	Generalised Mass (kg)			Natural Frequency (Hz)		
	(m)	(kg/m^2)	M_{MG}	M_{AG}	M_{MG+AG}	FE dry	FE wet	Exp.
1	0.0526	0.0645	0.001884	0.000834	0.002718	36.303	30.224	25.6
2	0.0326	0.0400	0.001196	0.000332	0.001528	58.595	51.840	48.8
3	0.0299	0.0366	0.001176	0.000300	0.001476	63.759	56.912	51.3
4	0.0282	0.0346	0.001113	0.000258	0.001371	67.679	60.980	62.0
5	0.0232	0.0284	0.001098	0.000218	0.001316	82.363	75.232	68.4
6	0.0216	0.0265	0.000835	0.000152	0.000987	88.255	81.175	80.0
7	0.0210	0.0257	0.000893	0.000161	0.001054	90.821	83.597	84.2
8	0.0201	0.0246	0.000867	0.000147	0.001014	94.933	87.782	87.3
9	0.0192	0.0235	0.000934	0.000149	0.001083	99.219	92.141	91.6
10	0.0181	0.0222	0.001069	0.000164	0.001233	105.75	98.466	94.0
11	0.0174	0.0213	0.001010	0.000150	0.001160	109.81	102.47	100.1
12	0.0167	0.0205	0.000968	0.000139	0.001107	114.51	107.08	105.0
13	0.0162	0.0199	0.001070	0.000148	0.001218	117.94	110.54	108.6
14	0.0159	0.0195	0.000633	0.000086	0.000719	120.06	112.65	113.5

Table 6.10 summarises the experimental and analytical results. In this model, there are no changes in the mode order.

Table 6.10: Vibration at 1 atm with 20 N/m surface tension with air on one side.

Mode	Natural Frequency (Hz)	
	Experimental	Analytical
1	25.6	30.22
2	48.8	51.84
3	51.3	56.91
4	62.0	60.98
5	68.4	75.23
6	80.0	81.18
7	84.2	83.60
8	87.3	87.78
9	91.6	92.14
10	94.0	98.47
11	100.1	102.47
12	105.0	107.08
13	108.6	110.54
14	113.5	112.65

Table 6.10 shows that for the lower modes the analytical natural frequencies are higher than the experimental frequencies, but for the higher modes the values are in good agreement.

(b) Air on the Two Sides of Membrane at 1 atm

Table 6.11 shows the calculation steps for the model with 1 atm pressure and 20 N/m surface tension; a summary of key results is given in Table 6.12.

Table 6.11: Vibration at 1 atm with 20 N/m surface tension with air on two sides.

Mode	$1/k_s$	m_a	Generalised Mass (kg)			Natural Frequency (Hz)		
	(m)	(kg/m^2)	M_{MG}	M_{AG}	M_{MG+AG}	FE dry	FE wet	Exp.
1	0.0526	0.1290	0.001884	0.001668	0.003552	36.303	26.439	25.6
2	0.0326	0.0800	0.001196	0.000664	0.001860	58.595	46.986	48.8
3	0.0299	0.0732	0.001176	0.000600	0.001776	63.759	51.883	51.3
4	0.0282	0.0692	0.001113	0.000516	0.001649	67.679	55.602	62.0
5	0.0232	0.0568	0.001098	0.000436	0.001534	82.363	69.682	68.4
6	0.0216	0.0530	0.000835	0.000304	0.001139	88.255	75.565	80.0
7	0.0210	0.0514	0.000893	0.000322	0.001215	90.821	77.862	84.2
8	0.0201	0.0492	0.000867	0.000294	0.001161	94.933	82.037	87.3
9	0.0192	0.0470	0.000934	0.000298	0.001232	99.219	86.390	91.6
10	0.0181	0.0444	0.001069	0.000328	0.001397	105.75	92.506	94.0
11	0.0174	0.0426	0.001010	0.000300	0.001310	109.81	96.420	100.1
12	0.0167	0.0410	0.000968	0.000278	0.001246	114.51	100.93	105.0
13	0.0162	0.0398	0.001070	0.000296	0.001366	117.94	104.38	108.6
14	0.0159	0.0390	0.000633	0.000172	0.000805	120.06	106.46	113.5

Table 6.12: Vibration at 1 atm with 20 N/m surface tension with air on two sides.

Mode	Natural Frequency (Hz)	
	Experimental	Analytical
1	25.6	26.44
2	48.8	46.99
3	51.3	51.88
4	62.0	55.60
5	68.4	69.68
6	80.0	75.56
7	84.2	77.86
8	87.3	82.04
9	91.6	86.39
10	94.0	92.51
11	100.1	96.42
12	105.0	100.93
13	108.6	104.38
14	113.5	106.46

Table 6.12 shows that now the analytical natural frequencies are less than the experimental frequencies for the higher modes, but for lower modes there is good agreement.

6.4 Discussion

The experimental and numerical nodal line patterns of the corresponding mode shapes (Figures 6.1 and 6.2) in vacuum are almost identical. This shows that the vacuum chamber test in Sewall et al. [35] is reliable.

The results tabulated in Table 6.2, for vibration at 0.61 atm under 93.4 N apex tension with air on one side of the membrane only, show a good similarity between experimental and analytical results. But, the results tabulated in Table 6.4 with air on both sides of the membrane which, of course, is a much more accurate representation of reality shows lower values for the analytical frequencies. Tables 6.6 and 6.8 for the same model at 1 atm with 93.4 N apex tension present exactly the same pattern.

The results tabulated in Table 6.10, for our own model of Chapter 5 with air on one side of the membrane show that for lower modes the analytical frequencies are higher than the experimental frequencies and for higher modes the values are in good agreement. But, the results tabulated in the Table 6.12 for the same model with air on two sides of the membrane show the opposite trend.

It is obvious from the above two model results that the prediction method does not

give the same pattern of results for the air-structure interaction problems. There are several reasons for the inconsistent behaviour of the approximate analytical prediction results. First, the air mass used in the prediction method is suitable for an infinite flat membrane lying on an infinite baffle. But, both experimental models have finite size. Second, the air mass expression is an approximate solution. Therefore, further work is needed to find out a suitable analytical expression for the air mass effect on the finite membranes.

Chapter 7

Conclusion

7.1 Discussion

7.1.1 Flat Membrane

A numerical and experimental study of the vibration of a flat membrane has been undertaken. Air effects on the vibration of the membrane have been revealed from the studies.

The numerical study conducted in ABAQUS, by applying membrane prestress as an initial stress, gives results similar to available analytical results. This study indicates that ABAQUS can be confidently used for vibration simulations of any membrane structures, by specifying the membrane prestress as an initial stress. Also, four node membrane elements (M3D4) have been found to be accurate.

An experimental study has been carried out on a triangular-shaped flat membrane to find its natural frequencies and mode shapes. The experimental natural frequencies have been obtained using an impulse technique and slow sine sweep method. Both experimental methods gave similar results for the natural frequencies. But, the experimental results for the natural frequencies were significantly lower than the numerical result obtained by using ABAQUS. The difference between these results indicates the effect of the surrounding medium on the membrane vibration.

The air-structure interaction in the vibration of a flat membrane has been studied. An approximate analytical method to predict the effect of air on the membrane vibration has been derived. The prediction method is capable of finding the natural frequencies and corresponding mode shapes for any air pressures. The prediction method has been checked with experimental results available in Sewall et al. [35] and in Chapter 5.

The predicted results for Sewall et al.'s model show a good agreement with the experimental results [35] when the air is assumed—"incorrectly"—to be only on one side of the membrane. The results are less accurate when the air is assumed to be on both sides of the membrane. It is observed that in air the sequence of the vibration modes changes from the order in vacuum.

The analytical results of the experimental model in Chapter 5 with air on one side of the membrane show that for the lower modes the analytical frequencies are higher than the experimental frequencies and in the higher modes both values are similar. But, the predicted analytical results of the same model with air on the two sides of the membrane show the opposite behaviour. Clearly, the approximate prediction method does not give the accurate air mass participating in vibration with this membrane model in either cases of air mass assumption. Because this model is physically smaller than Sewall et al.'s model, the sequence of the vibration modes has not changed from the order in vacuum.

The approximate prediction method does not give the same pattern of results as our own experimental model and Sewall et al.'s. The following reasons may have caused the lack of agreement between mode shapes in the two models. First, in the the membrane model, the membrane was modelled in ABAQUS as a triangle with curved edges, but in the experimental model it was not. Next, the experimental model in chapter 5 was too small to extract the accurate natural frequencies. Finally, Sewall et al.'s model has a lighter surface density than the experimental model.

7.1.2 CRTS Reflector

A numerical study of the vibration behaviour of CRTS reflectors has been done. The natural frequency increases with the number of ribs, although slight variations are observed in a few cases. As expected, the natural frequency decreases with the diameter of the reflector.

one important common feature that has been observed is that the existence of two different modes at a given natural frequency. It has also be observed that the number of normal modes in a given propagation zone equal to the number of ribs. But, the number of natural frequencies is less than the number of normal modes. This clearly shows the periodic nature of the reflector.

It can also be concluded that the increment in hub dimension does not have any effects on either the natural frequency or the periodicity of the reflector.

As expected, frequency increases with the increase of prestress. The increase of frequency is less for lower modes than for higher modes. The periodic behaviour of the reflector is observed as earlier.

7.2 Further Work

It was discussed in the previous section that the approximate prediction method does not give the same pattern of results for different models. Therefore, the prediction method needs to be revised.

It was observed that the CRTS reflector shows the periodic nature. Periodic structures have the advantage of simplifying dynamic analysis. But in reality, almost every practical structures have a small irregularities because of manufacturing and material tolerance. The structural irregularities can affect the vibration behaviour of nearly periodic structures significantly by localising the vibration modes and confining the energy to a region close to the source. The mode localisation in the CRTS reflector can cause the numerical predictions of the natural frequencies and the mode shapes to be completely incorrect. Therefore an experimental analysis of the CRTS reflector needs to be done.

Bibliography

[1] Blevins, A. *Formulas for Natural Frequencies and Mode shapes.* Krieger Publishing Company, USA, 1995.

[2] Clough, R. W., and Penzien, J. *Dynamics of Structures.* McGraw-Hill, Inc, 1993.

[3] Cook, R. D., Malkus, D. S., and Plesha, M. E. *Concepts and Applications of Finite Element Analysis.* John Wily & Sons, New York, USA, 1989.

[4] Cornwell, P. J., and Bendiksen, O. O. Localization of vibrations in large space reflectors. *AIAA Journal 27*, 2 (1989), 219–226.

[5] Craig, R. R. *Structural Dynamics.* John Wiley and Sons, 1981.

[6] Crighton, D. G. Approximations to the admittances and free wave numbers of fluid-loaded panels. *Journal of Sound and Vibration 68*, 1 (1980), 15–33.

[7] Crighton, D. G. The modes resonance and forced response of elastic structures under heavy fluid loading. *Philosophical Transaction of Royal Society of London A 312* (1984), 295–341.

[8] Crighton, D. G. The 1988 Raleigh medal lecture: Fluid loading—the interaction between sound and vibration. *Journal of Sound and Vibration 133*, 1 (1989), 1–27.

[9] Dungar, R. An efficient method of fluid-structure coupling in the dynamic analysis of structures. *International Journal for Numerical Methods in Engineering 13* (1978), 93–107.

[10] Everstine, G. C. Treatment of static preload effects in acoustic radiation and scattering. In *Proceeding of 16th NASTRAN user's Colloquium* (1988), pp. 138–152.

[11] Everstine, G. C., and Henderson, F. M. Coupled finite element/boundary element approach for fluid-structure interaction. *Journal of Acoustic Society of America 87*, 5 (1989), 1938–1947.

[12] Ewins, D. J. *Model Testing: Theory and Practice.* Research Studies Press Ltd., England, 1986.

[13] Fowler, J., Lagerquist, N., and Leve, H. Effect of air mass on modal tests. In *Proceedings of 5th International Modal Analysis Conferences* (1987), pp. 1078–1083.

[14] Graff, K. F. *Wave motion in elastic solids.* Clarendon Press, Oxford, 1975.

[15] Halvorsen, W. G., and Bandat, J. S. Noise source identification using coherent output power spectra. *Sound and Vibration 9*, 8 (1975), 15–24.

[16] Halvorsen, W. G., and Brown, D. L. Impulse technique for structural frequency response testing. *Sound and Vibration 11* (1977), 8–21.

[17] Hibbit and Karlsson and Sorensen, Inc. *ABAQUS/Standard User's Manuals, Version 5.8.* USA, 1998.

[18] Hrennikoff, S. Solution of problems of elasticity by the framework method. *Journal of Applied Mechanics, Transactions of the ASME 8* (1941), 169–175.

[19] Junger, M. C. Normal modes of submerged plates and shells. In *symposium on fluid-solid interaction* (1967), ASME, pp. 79 – 119.

[20] Junger, M. C., and Feit, D. *Sound, Structures, and their Interaction.* MIT Press, Cambridge, Massachusetts, 1986.

[21] King, S. A. *Nonlinear and Chaotic Dynamics of Thin-Walled Open-Section Deployable Structures.* PhD thesis, University of Cambridge, 1998.

[22] Lai, C. Y. Shape and stress analysis of edge-tensioned membranes. MPhil Thesis, University of Cambridge, 1997.

[23] Lai, C. Y., You, Z., and Pellegrino, S. Shape and stress analysis of crts reflectors. Tech. Rep. CUED/D-STRUCT/TR 170, University of Cambridge, 1997.

[24] Lai, C. Y., You, Z., and Pellegrino, S. Shape of deployable membrane reflectors. *Journal of Aerospace Engineering 11*, 3 (1998), 73–80.

[25] MacNeal-Schwedler Corporation, Inc. *MSC/PATRAN, Version 8.5.* USA, 1999.

[26] Mathews, I. C. Numerical technique for three-dimensional steady-state fluid-structure interaction. *Journal of Acoustic Society of America 79*, 5 (1986), 1317–1325.

[27] MathWorks, Inc. *Matlab user's Manual, Version 5.3.* USA, 1999.

[28] Miura, K., and Pellegrino, S. *Structural Concepts.* Cambridge University Press, Cambridge. (To Appear).

[29] Nour-Omid, B. Applications of the Lanczos method. *Computer Physics Communications 53* (1989), 157–168.

[30] Phaal, R. *A two-surface computational model for the analysis of thin shell structures.* PhD thesis, University of Cambridge, 1990.

[31] Rayleigh, J. W. S. *Theory of Sound*, vol. 1. Dover Publications, Inc., New York, 1945.

[32] Rits, W. J. A multipurpose deployable membrane reflector. *ESA Bulletin 88* (1996), 66–71.

[33] SenGupta, G. Natural flexural waves and the normal modes of periodically-supported beams and plates. *Journal of Sound and Vibration 13*, 1 (1970), 89–101.

[34] SenGupta, G. Vibration of periodic structures. *Shock and Vibration Digest 12*, 3 (1980), 17–31.

[35] Sewall, J. L., Miserentino, R., and Pappa, R. S. Vibration studies of a lightweight three-sided membrane suitable for space application. *NASA Technical Paper*, 2095 (1983).

[36] Smith, J. D. *Vibration Measurement and Analysis.* Butterworths & Co. Ltd., Great Britain, 1989.

[37] Sygulski, R. Dynamic analysis of open membrane structures interacting with air. *International Journal for Numerical Methods in Engineering 37* (1994), 1807–1823.

[38] Yap, D., and Cebon, D. Energy confinement in imperfect periodic systems. *Journal of Sound and Vibration 232*, 4 (2000), 669–694.

[39] Yasaka, T., and Oda, S. Air effects on the structure vibration and the considerations to large spacecraft ground testing. In *39th Congress of the International Astronautical Federation, IAF-88-291* (1988).

[40] You, Z. *Deployable Structures for Mast and Reflector Antennae.* PhD thesis, University of Cambridge, 1994.

Appendix A

A Sample ABAQUS Script

The following ABAQUS script was written to find out the fundamental natural frequency of the flat membrane shown in Figure 3.2 by using membrane elements.

```
*HEADING
MEMBRANE
Units: N m kg
*NODE
1, 0.0, 0.0, 0.0
11, 0.100, 0.0, 0.0
201, 0.0, 0.100, 0.0
211, 0.100, 0.100, 0.0
*NGEN, NSET=A1
1, 11, 1
*NGEN, NSET=A2
201, 211, 1
*NSET, NSET=A3, GENERATE
1, 201, 20
*NSET, NSET=A4, GENERATE
11, 211, 20
*NFILL
A1, A2, 10, 20
*ELEMENT, TYPE=M3D4
1, 1, 2, 22, 21
*ELGEN, ELSET=B1
1, 10, 1, 1, 10, 20, 10
*MEMBRANE SECTION, ELSET=B1, MATERIAL=KEVLAR
1E-4
*MATERIAL, NAME=KEVLAR
*DENSITY
790
```

```
*ELASTIC, TYPE=ISOTROPIC
11.9E9, 0.3
*INITIAL CONDITIONS, TYPE=STRESS
B1, 10E4, 10E4
*RESTART, WRITE
*STEP, NLGEOM
*STATIC
*BOUNDARY
A2, ENCASTRE
A4, ENCASTRE
A1, ENCASTRE
A3, ENCASTRE
*EL PRINT,POSITION=INTEGRATION POINT,FREQ=0
*EL FILE, FREQ=0,POSITION=INTEGRATION POINT
*NODE FILE, FREQ=0
*NODE PRINT, FREQ=0
*END STEP
*STEP
*FREQUENCY, EIGENSOLVER=LANCZOS
1
*BOUNDARY, OP=NEW
A1, 2
A3, 1
A4, 3
A2, 3
1, 1, 2
*EL PRINT, POSITION=INTEGRATION POINT, FREQUENCY=0
*EL FILE, FREQ=0,POSITION=INTEGRATION POINT
*NODE FILE, FREQ=0
*NODE PRINT, FREQ=0
*END STEP
```